

Abstract

During transport by advection, atmospheric nonspherical particles, such as volcanic, desert dust or sea-salt particles experience several chemical and physical processes, leading to a complex vertical atmospheric layering at remote sites where intrusion episodes occur. In this contribution, a new methodology is proposed to analyze this complex vertical layering in the case of a two / three-component particle external mixtures after long-range transport. This methodology relies on a precise analysis of the spectral and polarization properties of the light backscattered by atmospheric particles. It is based on combining a sensitive and accurate UV-VIS polarization Lidar experiment with accurate T-matrix numerical simulations and air mass back-trajectories. The Lyon UV-VIS polarization Lidar is used to efficiently partition the particle mixture into its nonspherical components, while the T-matrix algorithm is used for computing backscattering and depolarization properties specific to nonspherical volcanic, desert dust and sea-salt particles, the latter being described in the cubic shape approximation. It is shown that, after long-range transport, the particle mixtures' depolarization ratio δ_p differs from the nonspherical particles' depolarization ratio δ_{ns} due to the presence of spherical particles in the mixture. Hence, after identifying a tracer for nonspherical particles, particle backscattering coefficients specific to each nonspherical component can be retrieved in a two component external mixture. For three-component mixtures, the spectral properties of light must in addition be addressed by using a dual-wavelength polarization Lidar. Hence, for the first time, in a three-component external mixture, the nonsphericity of each particle is taken into account in a so-called $2\beta + 2\delta$ formalism. Applications of this new methodology are then demonstrated in two case studies carried out in Lyon, France, related to the mixing of Eyjafjallajökull volcanic ash with sulphate particles (case of a two-component mixture) and to the mixing of dust with sea-salt and water-soluble particles (case of a three-component mixture). This new methodology, which is able to provide separate vertical profiles of mixed atmospheric dust, sea-salt and water-soluble particles, may be useful for accurate radiative forcing assessments.

Retrieving volcanic, desert dust, and sea-salt particle properties

G. David et al.

Title Page

Abstract

Introduction

Conclusions

References

Tables

Figures

⏪

⏩

◀

▶

Back

Close

Full Screen / Esc

Printer-friendly Version

Interactive Discussion



1 Introduction

Atmospheric particles play an important role on the Earth's radiative budget and climate (Ramaswamy et al., 2001). As underlined in the IPCC report (2007), for climate forcing assessments, both particles and the gas molecules influence radiation. Gas molecules are the subject of many studies (Ehret et al., 2008; Stiller et al., 2012; Thomas et al., 2012) to quote only a few recent ones. The role of particles must be quantitatively estimated. This is a challenging task, in part due to the complexity of atmospheric particles, presenting a wide range of sizes, shapes and chemical compositions with interconnected distributions, as we recently published in a comprehensive study (Dupart et al., 2012). In particular, the particle nonsphericity is known to have a major impact on both lidar and satellite remote sensing retrievals (Mishchenko et al., 1995; Winker et al., 2009; 2010; Vernier et al., 2011). Remote sensing is a major source of global data on aerosol particle distributions needed in radiative and climate forcing assessments. Hence the lack of knowledge on volcanic ash, desert dust or sea-salt particles induces large uncertainties on the Earth's climate. This issue is also of fundamental importance since there is no generic, exact light scattering theory for nonspherical particles for which the century-old Lorentz-Mie formalism is not applicable (Mishchenko et al., 2000; Kahnert 2003). Additionally, atmospheric nonspherical particles may remain in the troposphere for several weeks (Robock, 2000; Overnevaide et al., 2009), which further reinforce their radiative impact. Hence, these particles are generally observed also at remote sites, far away from their source regions. During transport by advection from source regions to places where intrusion episodes occur, these particles experience several potential modifications, such as sedimentation, mixing with other particles (Zhang, 2008), hygroscopic growth and possible chemical alteration (Riccobono et al., 2011; Bourcier et al., 2011). Hence, after long-range transport, these particles are highly dispersed and aged, and may present sizes or shapes different from those observed in the source region. One of the consequences is a complex vertical layering generally observed in the low troposphere at far-range remote sites.

Retrieving volcanic, desert dust, and sea-salt particle properties

G. David et al.

Title Page

Abstract

Introduction

Conclusions

References

Tables

Figures



Back

Close

Full Screen / Esc

Printer-friendly Version

Interactive Discussion



Retrieving volcanic, desert dust, and sea-salt particle propertiesG. David et al.

[Title Page](#)[Abstract](#)[Introduction](#)[Conclusions](#)[References](#)[Tables](#)[Figures](#)[⏪](#)[⏩](#)[◀](#)[▶](#)[Back](#)[Close](#)[Full Screen / Esc](#)[Printer-friendly Version](#)[Interactive Discussion](#)

Lidar remote sensing is a very powerful instrument to provide vertical profiles of particles' backscattering properties under different atmospheric conditions of temperature and relative humidity. As explained by Mishchenko et al. (2002), atmospheric nonspherical particles can be detected by their ability to depolarize laser light. Using a single laser wavelength (1λ -polarization Lidar experiment) or several (for example, 2λ -polarization Lidar experiment), the depolarization of light by atmospheric particles has thus been studied in the backscattering direction, which is one of the most sensitive directions to many physical particle properties (Sugimoto et al., 2002; Sassen et al., 2007; Gasteiger et al., 2011; Miffre et al., 2011; Di Girolamo et al., 2012; David et al., 2012). As first proposed by Sasano and Browell (1989), 2λ -polarization Lidar experiments are often used to retrieve Angstrom exponents that describe the spectral dependence of atmospheric particles' backscattering coefficients. While depolarization measurements are often performed at visible (VIS) and infra-red (IR) spectral ranges (Sugimoto et al., 2002; Winker et al., 2009; Ansmann et al., 2011), at the ultra-violet (UV) spectral range polarization measurements are rather rare (Freudenthaler et al., 2009; Miffre et al., 2012a), especially in the low troposphere, as a consequence of strong UV-molecular scattering. As shown by David et al. (2012), to achieve sensitive and accurate particle UV-polarization Lidar measurements, a precise design and optimization of the Lidar detector is needed, to efficiently reduce possible systematic biases, allowing absolute particle UV-depolarization ratios as low as 6×10^{-3} , close to the UV-molecular depolarization, to be measured after precise polarization calibration (Alvarez et al., 2006) and significant solar background reduction (David et al., 2012). To complement these experimental studies, in the absence of exact light scattering theory for nonspherical particles, controlled numerical simulations have been performed to mimic the optical properties of nonspherical particles using spheroids (Nousiainen and Vermeulen, 2003; Dubovik et al., 2006; Nousiainen et al., 2006; Wiegner et al., 2009; Veselovskii et al., 2010) and more complex shapes (Nousiainen et al., 2009; Lindqvist et al., 2011) to quote only a few references. In addition, laboratory scattering matrix

measurements have been performed on volcanic ash (Muñoz et al., 2004), desert dust (Volten et al., 2001) and sea-salt particles (Sakai et al., 2010).

Depolarization of light by atmospheric nonspherical particles is particularly interesting to study after long-range transport, where the dependence of the depolarization on the wavelength has to be characterized (Wiegner et al., 2011) and fewer studies have been performed. During long-range transport, atmospheric nonspherical (ns) particles may mix with spherical (s) particles (case of a *two-component particles mixture*) or, additionally, with some other nonspherical particles (case of a *three-component particles mixture*). Example of a two-component mixture is given by the recent eruption of the Eyjafjallajökull volcano where volcanic ash particles mixed with spherical sulphate particles. Three-component mixture examples occur, for example, after Saharan dust outbreaks during which some nonspherical sea-salt particles may mix with desert dust particles and water-soluble species. Another example is given by the 2011 eruption of the Eritrean Nabro volcano, where volcanic ash particles encountered desert dust particles in the troposphere while also water soluble particles were present. In such situations, for radiative forcing assessments, the particle nonsphericity of sea-salt, desert dust and volcanic ash particles should be accounted for in the analysis. *Two-component particle mixtures* were first studied by Shimizu et al. (2004), who separated dust from non-dust particles using a 1λ -polarization Lidar system. This methodology was then applied by Tesche et al. (2009) to address the particle extinction at Raman channels, then further developed by Ansmann et al. (2012), assuming coarse particles (with diameter above $1\ \mu\text{m}$) to depolarize laser light while fine particles were assumed spherical (with diameter below $1\ \mu\text{m}$). This assumption seems questionable as dust particle diameters as low as 200 nanometres have been measured during SA-MUM field campaign (Kaaden et al., 2009). *Three-component particle mixtures* have been studied very recently by Nishizawa et al. (2011), who addressed nonspherical dust particles mixed with sea-salt and water-soluble particles, with a 1λ -polarization Lidar experiment (so-called $2\beta + 1\delta$ Lidar configuration). In that study, sea-salt particles were assumed to be spherical, which may not be the case, as first shown by

Retrieving volcanic, desert dust, and sea-salt particle properties

G. David et al.

[Title Page](#)[Abstract](#)[Introduction](#)[Conclusions](#)[References](#)[Tables](#)[Figures](#)[⏪](#)[⏩](#)[◀](#)[▶](#)[Back](#)[Close](#)[Full Screen / Esc](#)[Printer-friendly Version](#)[Interactive Discussion](#)

Murayama et al. (1999). Hence, to our knowledge, 2λ -polarization Lidar experiments have only been used to observe two-component particle mixtures (Sugimoto and Lee, 2006; Tesche et al., 2009).

In this Special Issue on the depolarization of light by atmospheric particles, polarization Lidar measurements have been performed on polar stratospheric clouds (Cordonà-Jabonero et al., 2012) while numerical simulations are proposed to study the depolarization of light by ice circular cylinders and their separation from spherical water droplets (Nicolet et al., 2012). Laboratory measurements have been performed for studying small ice crystals (Schnaiter et al., 2012) and dust particles (Glen et al., 2012). Our contribution combines sensitive and accurate 2λ -polarization Lidar measurements with accurate numerical simulations. The objective of this paper is to show what is objectively retrievable when combining these two methodologies, as opposed to comparing both approaches separately, as is often presented in the literature. More precisely, this contribution is dedicated to the polarization (π) and spectral (λ) properties of atmospheric nonspherical particles after long-range transport. In particular, we study the depolarization of UV-VIS light by a three-component external mixture of particles, to be chosen between volcanic ash, desert dust, sea-salt or water soluble particles. As shown below, the complex vertical layering observed at far-range remote sites can hence be partitioned by precisely analyzing the polarization of backscattered photons (David et al., 2012) after long-range transport. We here develop a new methodology to retrieve, from a three-component particle mixture, range-resolved vertical profiles of atmospheric particles' backscattering coefficients, specific to each particle component. This new methodology relies on the combined use of a sensitive and accurate 2λ -polarization Lidar experiment ($2\beta + 2\delta$ Lidar configuration) and accurate T-matrix numerical simulations, the latter being necessary to specifically address nonspherical particles in the three-component particles mixture. The coupling of Lidar with inelastic Raman scattering (Müller et al., 2001) as well as with passive remote sensing (Dubovik et al., 2006; Boyouk et al., 2011), has not been considered in this paper. A precise chemical analysis has not been performed during the experiments carried

Retrieving volcanic, desert dust, and sea-salt particle properties

G. David et al.

Title Page

Abstract

Introduction

Conclusions

References

Tables

Figures



Back

Close

Full Screen / Esc

Printer-friendly Version

Interactive Discussion

out, because it is not the scope of this contribution. We hence used 7-days air mass back-trajectories to identify the origin of the nonspherical particles at the remote site. Otherwise, the combined use of our Lidar depolarization experiment with laboratory chemical studies has been already published Dupart et al. (2012). Here, for the first time, a three-component particles mixture is partitioned by using a 2λ -polarization Lidar (development of a $2\beta + 2\delta$ algorithm) to take into account the particle nonsphericity within each component. Moreover, the spectral behavior of the retrieved backscattering coefficients is considered.

The paper is organized as follows. Section 2 is devoted to the detailed description of our methodology. Polarization Lidars rely on the scattering matrix formalism, here shortly summarized to introduce our notations and to define the particles' Lidar backscattering coefficient β_p and depolarization ratio δ_p . Then, depolarization of light by a two, then a three-component particle mixture is studied. It is shown that after long-range transport, despite s-particles not being able to depolarize backscattered laser light, they contribute to the depolarization ratio δ_p of the particle mixture by lowering the depolarization ratio δ_{ns} that would be observed in the absence of s-particles. Hence, and as a first result, the maximum observed δ_p -value cannot be used as a δ_{ns} -measurement. A tracer for ns-particles is then identified to retrieve the ns-particle backscattering coefficient β_{ns} for each component in a two, then a three-component particle mixture. By addressing the spectral behavior of the ns-particles' backscattering coefficient β_{ns} in a three-component mixture, we show how to retrieve vertical profiles of particles' backscattering properties, specific to one-component ns-particles. The 2λ -polarization Lidar experiment is then described in Sect. 3 where polarization-resolved particle backscattering profiles are retrieved, with special emphasis on our error bars, derived after accurately calibrated polarization measurements (David et al., 2012). The backscattering and depolarization properties of ash, dust and sea-salt particles are then separately addressed in Sect. 4, where controlled T-matrix numerical experiments on these ns-particles are performed. Section 5 is dedicated to the application of this new methodology in two case studies. Firstly, an example of a *two-component particles*

Retrieving volcanic, desert dust, and sea-salt particle properties

G. David et al.

Title Page

Abstract

Introduction

Conclusions

References

Tables

Figures

⏪

⏩

◀

▶

Back

Close

Full Screen / Esc

Printer-friendly Version

Interactive Discussion

mixture is analyzed, where Eyjafjallajökull volcanic ash particles mixed with spherical sulphate particles produced by SO₂-oxydation over Lyon (France) on April 2010, after more than 2600 km of advection transport. Then, the mixing of desert dust with sea-salt and water-soluble particles, – an example of a *three-component particles mixture* –, is analyzed during a long-range Saharan dust outbreak over Lyon which occurred in October 2011. For the first time, both sea-salt and dust particles are treated as non-spherical, which is justified in regards to the observed low relative humidity. We believe this new treatment may be used for precise radiative forcing assessments as well as satellite retrievals. The paper ends with conclusions and outlooks.

2 Methodology

In this section, we describe our methodology for Lidar retrievals of atmospheric ns-particles in *two or three-component particle external mixtures* after long-range transport. It is based on combining a 2λ-polarization Lidar with numerical simulations that specifically account for each ns-particle component in the particles mixing.

2.1 Particle microphysical properties

The nonsphericity of volcanic ash, desert dust and sea-salt particles is clearly visible in the electron microscope images presented in Table 1. Volcanic ashes and desert dust particles have highly irregular shapes. Sea-salt particles exhibit a cube-like shape below the 40 %-relative humidity crystallization point of sodium chloride (Randriamiarisoa et al., 2006). As shown by Wise et al. (2005), for relative humidity (RH) below this crystallization point, salt particles exhibit crystal faces, corresponding to effloresced particles, and the particle shapes remain unchanged as long as the 75 %-deliquescence point is not reached. Above the deliquescence point, salt particles present a non-cubic shape (Wise et al., 2005) and may be treated as spherical by applying the well-known Lorentz-Mie theory. By shape, we refer to the overall shape of the particles, different

Retrieving volcanic, desert dust, and sea-salt particle properties

G. David et al.

Title Page

Abstract

Introduction

Conclusions

References

Tables

Figures



Back

Close

Full Screen / Esc

Printer-friendly Version

Interactive Discussion



from the particles' morphology which would include internal structures and porosity effects (Nousiainen et al., 2012). Such a morphological study is beyond the scope of this paper. Here we limit to RH-values below the crystallization point, where the sea-salt cubic shape approximation is appropriate. Water-soluble (ws) particles are defined according to the classification of Hess et al. (1998) and include sulphate and nitrate particles as well as other organic water-soluble substances. An almost spherical ammonium sulphate particle is shown in Table 1. Due to particle hygroscopicity, these water-soluble particles tend to be spherical and will be treated as such. For each particle component, some literature references are also given in Table 1, on Lidar remote sensing studies as well as numerical simulations and laboratory experiments on their light-scattering properties. When different particle types are present, they are assumed externally mixed (Mishchenko, 2009). For example, volcanic ash particles are assumed externally mixed with sulphate particles, produced by SO₂-oxydation (Schumann et al., 2011). Likewise, when mixing sea-salt and desert dust particles, no internal mixture, such as pollutant-coated dust or internal mixture of sulphate and organic carbon is assumed. From now on, nonspherical particles (resp. spherical) will be abbreviated as ns-particles (resp. s-particles).

2.2 Theoretical considerations on light scattering by atmospheric particles

Here we present the polarization Lidar observables suitable for range-resolved experimental observations of ns-particles in the atmosphere in terms of the scattering matrix formalism. In particular, we emphasize what is meant by light depolarization by an ensemble of particles.

2.2.1 Scattering matrix formalism

Scattering of light by an ensemble of particles of arbitrary size, shape and chemical composition can be described by the scattering matrix formalism, which relates the Stokes vectors $[I, Q, U, V]^T$ of the incident (inc) and scattered (sca) light waves with

Retrieving volcanic, desert dust, and sea-salt particle properties

G. David et al.

Title Page

Abstract

Introduction

Conclusions

References

Tables

Figures



Back

Close

Full Screen / Esc

Printer-friendly Version

Interactive Discussion



respect to the laser scattering plane:

$$\begin{pmatrix} I_{\text{sca}} \\ Q_{\text{sca}} \\ U_{\text{sca}} \\ V_{\text{sca}} \end{pmatrix} = \frac{C_{\text{sca,p}}}{4\pi d^2} \begin{bmatrix} F_{11,p} & F_{12,p} & F_{13,p} & F_{14,p} \\ F_{21,p} & F_{22,p} & F_{23,p} & F_{24,p} \\ F_{31,p} & F_{32,p} & F_{33,p} & F_{34,p} \\ F_{41,p} & F_{42,p} & F_{43,p} & F_{44,p} \end{bmatrix} \begin{pmatrix} I_{\text{inc}} \\ Q_{\text{inc}} \\ U_{\text{inc}} \\ V_{\text{inc}} \end{pmatrix} \quad (1)$$

where the p-subscript refers to the particle, d is the distance between the particle and the observer and $C_{\text{sca,p}}$ is the scattering cross-section of the particle, which depends on the wavelength λ of the radiation and on the particle radius r . For an ns-particle, r is defined here as the volume equivalent radius, i.e. the radius of an s-particle having the same volume as the considered ns-particle. For numerical simulations (see Sect. 4), it is useful to introduce the size parameter $x = 2\pi r/\lambda$, which is dimensionless. The F_{ij} -matrix elements are function of the particles' size, shape and chemical composition, and depend on the scattering angle, on the size parameter x and on the complex refractive index m , through which absorption may occur. In this contribution, we only consider the quantities in the Lidar backscattering direction. Moreover, particles are assumed to be randomly oriented (see Nicolet et al., 2012 for a study of depolarization of light by horizontally oriented ice crystals). Following Mishchenko and Hovenier (1995), the backscattering matrix is diagonal and depends only on $F_{11,p}$ and $F_{22,p}$. At distances large compared to the particles' size, and for a perfectly linearly polarized incident light, – i.e. as for polarization Lidar experiments –, the backscattered light wave is then given by:

$$\begin{pmatrix} I_{\text{sca,//}} + I_{\text{sca,\perp}} \\ I_{\text{sca,//}} - I_{\text{sca,\perp}} \\ 0 \\ 0 \end{pmatrix} = \frac{C_{\text{sca,p}}}{4\pi d^2} \begin{bmatrix} F_{11,p} & 0 & 0 & 0 \\ 0 & F_{22,p} & 0 & 0 \\ 0 & 0 & -F_{22,p} & 0 \\ 0q & 0 & 0 & F_{11,p} - 2F_{22,p} \end{bmatrix} \begin{pmatrix} 1 \\ 1 \\ 0 \\ 0 \end{pmatrix} \quad (2)$$

where $\pi = \{/, \perp\}$ polarization components are, respectively, called the co- and cross-polarized polarization components with respect to the incident laser linear polarization.

Retrieving volcanic, desert dust, and sea-salt particle properties

G. David et al.

Title Page

Abstract

Introduction

Conclusions

References

Tables

Figures

⏪

⏩

◀

▶

Back

Close

Full Screen / Esc

Printer-friendly Version

Interactive Discussion

2.2.2 Polarization Lidar formalism

In the polarization Lidar formalism, the backscattered intensities $I_{\text{sca},//}$ and $I_{\text{sca},\perp}$ are measured separately with a polarization-sensitive detector. These intensities can be used to define co- and cross-polarized particle backscattering cross-sections, which depend on r , m and λ :

$$\left(\frac{d\sigma}{d\Omega}\right)_{\text{p},//}(r, m, \lambda) = d^2 \frac{I_{\text{sca},//}}{I_{\text{inc}}} = \frac{C_{\text{sca},\text{p}}}{4\pi} \left(\frac{F_{11,\text{p}} + F_{22,\text{p}}}{2}\right) \quad (3a)$$

$$\left(\frac{d\sigma}{d\Omega}\right)_{\text{p},\perp}(r, m, \lambda) = d^2 \frac{I_{\text{sca},\perp}}{I_{\text{inc}}} = \frac{C_{\text{sca},\text{p}}}{4\pi} \left(\frac{F_{11,\text{p}} - F_{22,\text{p}}}{2}\right) \quad (3b)$$

by using Eq. (2). Usually, a Lidar measures size-averaged particle backscattering cross-sections, which define the so-called volume particle backscattering coefficients (in $\text{Mm}^{-1}\text{sr}^{-1}$):

$$\beta_{\text{p},//}(\lambda) = \int_{\text{PSD}} \left(\frac{d\sigma}{d\Omega}\right)_{\text{p},//} n_{\text{p}}(r) dr = N_{\text{p}} \times \left\langle \left(\frac{d\sigma}{d\Omega_{\text{p}}}\right) \right\rangle_{//} \quad (4a)$$

$$\beta_{\text{p},\perp}(\lambda) = \int_{\text{PSD}} \left(\frac{d\sigma}{d\Omega}\right)_{\text{p},\perp} n_{\text{p}}(r) dr = N_{\text{p}} \times \left\langle \left(\frac{d\sigma}{d\Omega_{\text{p}}}\right) \right\rangle_{\perp} \quad (4b)$$

where the integration is performed over the particle size distribution (PSD) defined by the particle number density $n_{\text{p}}(r) = dN_{\text{p}}/dr$ for a particle number concentration N_{p} (in part m^{-3}). In contrast to ns-particles, s-particles, for which $F_{11,\text{s}} = F_{22,\text{s}}$, exhibit a null $\beta_{\text{p},\perp}$ coefficient. For the sake of clarity, we emphasize that the subscripts $\{//, \perp\}$ of β_{p} are relative to the polarization detector and defined with respect to the incident linear polarization and do not apply to atmospheric parameters (Gimmestad, 2008). The volume backscattering coefficient is additive and depends on the size, shape, λ

and m of the particles in the volume. It is linked to the scattering matrix formalism as follows:

$$\beta_p(\lambda) = \beta_{p, //}(\lambda) + \beta_{p, \perp}(\lambda) = \int_{\text{PSD}} \frac{C_{\text{sca}, p}}{4\pi} F_{11, p} n_p(r) dr = N_p \times \left\langle \left(\frac{d\sigma}{d\Omega_p} \right) \right\rangle \quad (5)$$

Backscattering thus occurs from both the s and ns-particles. Contrary to backscattering, extinction is not sensitive to polarization effects for randomly oriented particles. Here, the extinction will be characterized by the particles' extinction-to-backscatter ratio S_p defined as:

$$S_p(\lambda) = \alpha_p(\lambda)/\beta_p(\lambda) \text{ with } \alpha_p(\lambda) = \int_{\text{PSD}} C_{\text{ext}, p} n_p(r) dr \quad (6)$$

where $C_{\text{ext}, p}$ is the extinction coefficient of the particle. Moreover, the relative amount of power $I_{\text{sca}, \perp}/I_{\text{sca}, //}$ in the co- and cross-polarized polarization components is an often-used quantity in the Lidar community, known as the particles' linear depolarization ratio δ_p . By combining Eqs. (1), (2), for a particle with a radius r , δ_p is defined as follows:

$$\delta_p(r, \lambda) = \frac{I_{\text{sca}, \perp}}{I_{\text{sca}, //}} = \frac{I_{\text{sca}} - Q_{\text{sca}}}{I_{\text{sca}} + Q_{\text{sca}}} = \frac{F_{11, p} - F_{22, p}}{F_{11, p} + F_{22, p}} \quad (7)$$

Like $F_{11, p}$ and $F_{22, p}$, the δ_p -ratio depends on the shape, r , m and λ , and is non-additive. Equation (7) shows that s-particles do not depolarize laser light, in contrary to ns-particles for which the polarization state of the incident light is modified. This non-zero linear polarization change is called depolarization (Harris-Hobbs and Cooper, 1987; Baumgardner et al., 2012). These shape-dependent features arise in polarization-resolved backscattering from the interference of different parts of an anisotropic particle, although absorption may somewhat dampen this interference. Numerical simulations show that the magnitude of δ_p is not a clear indicator of the particles' overall

Retrieving volcanic, desert dust, and sea-salt particle properties

G. David et al.

Title Page

Abstract

Introduction

Conclusions

References

Tables

Figures

⏪

⏩

◀

▶

Back

Close

Full Screen / Esc

Printer-friendly Version

Interactive Discussion



shape or morphology (Nousiainen et al., 2012). However, as also demonstrated in this paper, it is a clear indicator for deviation from particle isotropy, and can be used to partition a mixture of particles into its s and ns-components, provided that sensitive and accurate polarization Lidar measurements are performed (see Sect. 3). In polarization Lidar experiments, the particles' depolarization ratio is integrated over the PSD, and hereafter noted $\delta_p(\lambda)$. By using Eq. (4), δ_p is equal to the ratio $\beta_{p,\perp}/\beta_{p,\parallel}$, as is well-known in the Lidar community.

2.3 Depolarization of light by a two-component particle mixture

After long-range transport, ns-particles, such as those presented in Table 1, experience chemical reactivity, including potential humidification during advection (Overnevaide et al., 2009; Schumann et al., 2011). At a place where intrusion episodes occur, the particles' external mixture is hence composed of both s and ns-particles. We here show how to specifically address ns-particles' backscattering in such a particle mixture by using a 1λ -polarization Lidar. In this subsection, to ease the reading, the λ -wavelength dependence is omitted.

2.3.1 Depolarization ratio of a {s, ns} particles mixing

Let us consider an external mixture of particles composed of both s and ns-particles, having a total depolarization ratio δ_p . The depolarization ratio of its ns-particles is denoted δ_{ns} . Since the δ_p -ratio is not additive, despite δ_s being zero, there is no reason for δ_p to equal δ_{ns} . Using the additive scattering matrix $\bar{F}_p = C_{sca,p} \times F_p / (4\pi)$, the mixture of particles has a scattering matrix $\bar{F}_p = \bar{F}_s + \bar{F}_{ns}$, sum of its s and ns-components. By developing this equation for the $F_{11,p}^-$ and $F_{22,p}^-$ matrix elements, noting that $F_{11,s}^- = F_{22,s}^-$, the δ_p -ratio of the particles mixture can be related to the depolarization ratio δ_{ns} of its

Retrieving volcanic, desert dust, and sea-salt particle properties

G. David et al.

[Title Page](#)[Abstract](#)[Introduction](#)[Conclusions](#)[References](#)[Tables](#)[Figures](#)[⏪](#)[⏩](#)[◀](#)[▶](#)[Back](#)[Close](#)[Full Screen / Esc](#)[Printer-friendly Version](#)[Interactive Discussion](#)

ns-particles as follows (Miffre et al., 2011):

$$\frac{1}{\delta_p} = \frac{1}{\delta_{ns}} + \frac{F_{11,s} + F_{22,s}}{F_{11,ns} - F_{22,ns}} \left(\frac{C_{sca,s}}{C_{sca,ns}} \right) \frac{N_s}{N_{ns}} \quad (8)$$

Hence, when s-particles are present – such as after long-range transport –, the δ_p -ratio of a {s, ns} particle mixture is lower than the depolarization ratio of its ns-particles ($\delta_p \leq \delta_{ns}$). Accordingly, the same conclusion can be drawn in the frame of the Lidar formalism by combining Eqs. (4a, b), (8):

$$\frac{1}{\delta_p} = \frac{1}{\delta_{ns}} + \frac{\beta_{s, //}}{\beta_{ns, \perp}} \quad (9)$$

In the literature, δ_p is often compared to δ_{ns} (Gasteiger et al., 2011) and the maximum value of δ_p is sometimes used as a δ_{ns} -measurement (Shimizu et al., 2004). Moreover, the difference between δ_p and δ_{ns} is not clearly stated to originate from the presence of s-particles, and the observed discrepancies between δ_p and δ_{ns} are sometimes attributed to imperfections originating from numerical simulations or/and experimental observations (Wiegner et al., 2009). Hence, identification of ns-particles from δ_p -measurements (Gross et al., 2011) is not appropriate for long-range transport studies. The scattering-matrix derived Eq. (8), or its Lidar-equivalent Eq. (9) show that δ_p equals δ_{ns} only when there are no s-particles present ($N_s = 0$), i.e. near the source region. Since we focus on long-range transport situations, s-particles are expected to be present in the particle mixtures and lower δ_p below δ_{ns} . As a consequence, after long-range transport, the backscattering properties of ns-particles in the {s, ns} particle mixtures cannot be easily derived from the Lidar-measured δ_p -value, because the latter is not a tracer specific to ns-particles only. A tracer for ns-particles can be derived from the Lidar formalism by applying the superposition principle to particle backscattering coefficient β_p , i.e. $\beta_p = \beta_s + \beta_{ns}$, assuming no interaction between s and ns-particles.

Retrieving volcanic, desert dust, and sea-salt particle properties

G. David et al.

Title Page

Abstract

Introduction

Conclusions

References

Tables

Figures

◀

▶

◀

▶

Back

Close

Full Screen / Esc

Printer-friendly Version

Interactive Discussion



On each $\pi = \{/, \perp\}$ polarization axis, we get:

$$\beta_{p, //} = \beta_{s, //} + \beta_{ns, //} \quad (10a)$$

$$\beta_{p, \perp} = \beta_{ns, \perp} \quad (10b)$$

5 Hence, even after long-range transport, only the cross-polarized particle backscattering coefficient $\beta_{p, \perp}$ is a tracer specific to ns-particles, in contrast to the δ_p -ratio or the $\beta_{p, //}$ -coefficient. Using Eq. (9b), the ns-particle backscattering coefficient β_{ns} can be expressed as a function of δ_{ns} :

$$\beta_{ns} = \beta_{ns, \perp} \left(1 + \frac{1}{\delta_{ns}} \right) \quad (11)$$

10 For accurate determination of β_{ns} , sensitive and accurate $\beta_{ns, \perp}$ -Lidar measurements (see Sect. 3), as well as accurate numerical simulations of δ_{ns} , are therefore necessary (see Sect. 4).

2.3.2 Fraction of ns-particles in the two-component particle mixture

To emphasize the contribution of s-particles to the δ_p -ratio, Eqs. (8) or (9) can be
 15 rewritten by introducing the fraction $X_{ns} = \beta_{ns} / \beta_p$ of ns-to-particle backscattering coefficients. By combining Eqs. (10) and (11), while noting that $\beta_s = \beta_{s, //}$ and $\beta_s = \beta_p - \beta_{ns}$, we get:

$$\frac{1}{\delta_p} = \frac{1}{\delta_{ns}} + \frac{1 - X_{ns}}{X_{ns}} \left(1 + \frac{1}{\delta_{ns}} \right) \quad (12)$$

Thus, the difference between δ_p and δ_{ns} can be used to determine the fraction X_{ns} of
 20 ns-particles in the two-component particles mixture:

$$X_{ns} = \frac{1 + \frac{1}{\delta_{ns}}}{1 + \frac{1}{\delta_p}} \approx \delta_p \left(1 + \frac{1}{\delta_{ns}} \right) \quad (13)$$

as long as $\delta_p \ll 1$, so that δ_p is a tracer for X_{ns} while δ_{ns} can be determined by following the procedure detailed in Sect. 4. Equation (13), derived from scattering matrix considerations, agrees with Tesche et al. (2009). Since δ_p is sometimes assumed to equal δ_{ns} , we plotted in Fig. 1 the systematic bias between δ_p and δ_{ns} as a function of X_{ns} for each ns-component (volcanic ashes, desert dust, sea-salt particles). The relative error is larger when δ_{ns} is larger but the three curves look almost independent on δ_{ns} . For a given X_{ns} value, the larger δ_{ns} is, the larger the bias between δ_p and δ_{ns} is. Hence, to quantify the ns-particle content X_{ns} in the atmosphere, sensitive and accurate polarization Lidar measurements are necessary (Sect. 3), as well as a precise numerical simulation of δ_{ns} (Sect. 4). The numerical simulations are exploited to separate the specific contribution of ns-particles. The needed assumptions are detailed in Sect. 4 and the influence of these assumptions is discussed in detail in Sect. 5.2. Moreover, to lower the X_{ns} -uncertainty, the lower δ_{ns} is, the more accurate the determination of δ_p must be.

2.3.3 Separate retrieval of particle backscattering coefficient in the external mixture

When the particles mixture (ρ) = {s, ns} enters the low troposphere, it often mixes with local aerosols such as ammonium sulphate, nitrate or carbonaceous soot aggregates present in the urban canopy (Miffre et al., 2010). To account for possible background depolarization, the particle mixture is preferably partitioned between ns (ash, dust, sea-salt) particles on the one hand, and non-ns particles, i.e. particles that are neither ash, dust nor sea-salt particles, on the other hand. In this practical case, to separately retrieve the ns and non-ns backscattering coefficients, we wrote the following set of

Retrieving volcanic, desert dust, and sea-salt particle properties

G. David et al.

[Title Page](#)[Abstract](#)[Introduction](#)[Conclusions](#)[References](#)[Tables](#)[Figures](#)[⏪](#)[⏩](#)[◀](#)[▶](#)[Back](#)[Close](#)[Full Screen / Esc](#)[Printer-friendly Version](#)[Interactive Discussion](#)

four equations:

$$\beta_{p, //} = \beta_{ns, //} + \beta_{non-ns, //} \quad (14a)$$

$$\beta_{p, \perp} = \beta_{ns, \perp} + \beta_{non-ns, \perp} \quad (14b)$$

$$\delta_{ns} = \beta_{ns, \perp} / \beta_{ns, //} \quad (14c)$$

$$\delta_{non-ns} = \beta_{non-ns, \perp} / \beta_{non-ns, //} \quad (14d)$$

Four backscattering coefficients are hence to be determined, namely $\beta_{p, \pi}$ with $(p) = \{ns, non-ns\}$ and $\pi = \{ //, \perp \}$. This is feasible by combining sensitive and accurate $\beta_{p, //}$ and $\beta_{p, \perp}$ -Lidar measurements with accurate δ_{ns} -numerical simulations, while δ_{non-ns} can be assumed to be equal to 1 % (Sakai et al., 2010). An application of this methodology is given in Sect. 5.1 (*case study 1*), where the mixing of volcanic ashes with spherical sulphate particles is studied to retrieve vertical profiles of β_{ash} , $\beta_{non-ash}$ and $X_{ash} = \beta_{ash} / \beta_p$.

2.4 Depolarization of light by a three-component particle mixture

The mixing of ns-particles with s-particles that occurs after long-range transport may concern two different ns-particles. We here present a new methodology, which consists in using a $2\beta+2\delta$ polarization Lidar together with numerical light-scattering simulations, to retrieve the particle backscattering coefficients of both ns-components in a three-component mixture. This section can be thought as an extension of Sect. 2.3 to a three-component mixture.

2.4.1 Introduction

In the three-component mixture, we label particles by their index, i.e. $(p) = \{ns1, ns2, n12\}$, where ns1 and ns2 refer to the two ns-particle populations (see Table 1), while n12-particles belong to neither ns1 nor ns2 particles. After long-range transport, the n12-population is composed of s-particles or water-soluble particles, and local aerosols

Retrieving volcanic, desert dust, and sea-salt particle properties

G. David et al.

Title Page

Abstract

Introduction

Conclusions

References

Tables

Figures

⏪

⏩

◀

▶

Back

Close

Full Screen / Esc

Printer-friendly Version

Interactive Discussion



such as sulphate or nitrate particles may also contribute to n12. In this paper, n12-particles are assumed spherical, so that water-soluble particles are simply assumed s-particles. For an external mixture of ns1, ns2 and n12-particles, following the same methodology as in Sect. 2.2, after long-range transport, n12-particles contribute to the δ_p -ratio of the three-component mixture and δ_p is below $\max(\delta_{ns1}, \delta_{ns2})$, where δ_{ns1} (resp. δ_{ns2}) is the ns1-particles' depolarization ratio (resp. ns2). As to be shown below, the X_{ns1} and X_{ns2} -fractions ($X_{ns} = \beta_{ns}/\beta_p$) can be determined from separate retrievals of {ns1, ns2, n12} backscattering coefficients, using both the 2λ -polarization Lidar experiment (see Sect. 3) and controlled numerical experiments (see Sect. 4).

2.4.2 Separate retrieval of {ns1, ns2, n12} backscattering in the three-component particle mixture

To determine the backscattering coefficients of ns-particles in the three-component mixture (p) = { ns1, ns2, n12}, six unknown quantities have to be determined, corresponding to the three components (ns1, ns2, n12) assigned to the two detector polarization axes $\pi = \{ //, \perp \}$. When dealing with a 2λ -polarization Lidar experiment ($2\beta + 2\delta$ Lidar configuration), each of these backscattering coefficients has to be determined at the two Lidar wavelengths $\lambda = \{\lambda_1, \lambda_2\}$. Hence, twelve unknown backscattering coefficients have to be determined, hereafter noted $\beta_{p,\pi}(\lambda)$.

As shown in Sect. 3, our 2λ -polarization Lidar experiments provide vertical profiles of co- and cross-polarized particles backscattering coefficient $\beta_{p, //}(\lambda)$ and $\beta_{p, \perp}(\lambda)$ at wavelength λ . By applying the superposition principle to the three-component mixture, for the (λ, π) spectral and polarization property, the $\beta_{p, //}(\lambda)$ and $\beta_{p, \perp}(\lambda)$ coefficients provide a set of four equations:

$$\beta_{p, //}(\lambda) = \beta_{ns1, //}(\lambda) + \beta_{ns2, //}(\lambda) + \beta_{n12, //}(\lambda) \quad (15a, b)$$

$$\beta_{p, \perp}(\lambda) = \beta_{ns1, \perp}(\lambda) + \beta_{ns2, \perp}(\lambda) + \beta_{n12, \perp}(\lambda) \quad (15c, d)$$

For the sake of clarity, we note that Eq. (15a, b) refers to λ_1 -wavelength, while Eq. (15c, d) refers to wavelength λ_2 . Six more equations are then provided by numerical simu-

Retrieving volcanic, desert dust, and sea-salt particle properties

G. David et al.

Title Page

Abstract

Introduction

Conclusions

References

Tables

Figures

◀

▶

◀

▶

Back

Close

Full Screen / Esc

Printer-friendly Version

Interactive Discussion



lations by computing the ns-particle depolarization ratio at the two Lidar wavelengths $\lambda = \{\lambda_1, \lambda_2\}$:

$$\delta_{ns1}(\lambda) = \beta_{ns1,\perp}(\lambda)/\beta_{ns1,//}(\lambda) \quad (15e, f)$$

$$\delta_{ns2}(\lambda) = \beta_{ns2,\perp}(\lambda)/\beta_{ns2,//}(\lambda) \quad (15g, h)$$

$$5 \quad \delta_{n12}(\lambda) = \beta_{n12,\perp}(\lambda)/\beta_{n12,//}(\lambda) \quad (15i, j)$$

The last two equations are obtained by addressing the spectral behavior of the backscattering coefficient β_{ns} . By using Eq. (4a, b), we may write:

$$\frac{\beta_{ns1,\perp}(\lambda_2)}{\beta_{ns1,\perp}(\lambda_1)} = \left\langle \left(\frac{d\sigma}{d\Omega} \right)_{ns1,\perp}(\lambda_2) \right\rangle / \left\langle \left(\frac{d\sigma}{d\Omega} \right)_{ns1,\perp}(\lambda_1) \right\rangle \quad (15k)$$

$$10 \quad \frac{\beta_{ns2,\perp}(\lambda_2)}{\beta_{ns2,\perp}(\lambda_1)} = \left\langle \left(\frac{d\sigma}{d\Omega} \right)_{ns2,\perp}(\lambda_2) \right\rangle / \left\langle \left(\frac{d\sigma}{d\Omega} \right)_{ns2,\perp}(\lambda_1) \right\rangle \quad (15l)$$

where the average is performed over the ns-particle size distribution (PSD). Equation (15k), (15l) hold provided that, in the Lidar experiment, the same atmospheric volume is probed at both wavelengths, as justified in Sect. 3. Hence, when dealing with a 2λ -polarization Lidar experiment, the twelve unknown backscattering coefficients $\beta_{p,\pi}(\lambda)$ can be determined from the twelve equations system (Eq. 15). As a conclusion, by applying Eq. (10), vertical profiles of $\beta_{p,\pi}(\lambda)$ can be retrieved for each particle component (p) = {ns1, ns2, n12} at wavelength λ_1 and λ_2 :

$$\beta_{ns1}(\lambda) = \beta_{ns1,//}(\lambda) + \beta_{ns1,\perp}(\lambda) \quad (16a, b)$$

$$20 \quad \beta_{ns2}(\lambda) = \beta_{ns2,//}(\lambda) + \beta_{ns2,\perp}(\lambda) \quad (16c, d)$$

$$\beta_{n12}(\lambda) = \beta_{n12,//}(\lambda) + \beta_{n12,\perp}(\lambda) \quad (16e, f)$$

To apply this new methodology, sensitive and accurate 2λ -polarization Lidar measurements, to be detailed in Sect. 3, must be performed to determine vertical profiles of

Retrieving volcanic, desert dust, and sea-salt particle properties

G. David et al.

Title Page

Abstract

Introduction

Conclusions

References

Tables

Figures

⏪

⏩

◀

▶

Back

Close

Full Screen / Esc

Printer-friendly Version

Interactive Discussion



Retrieving volcanic, desert dust, and sea-salt particle properties

G. David et al.

Title Page

Abstract

Introduction

Conclusions

References

Tables

Figures

◀

▶

◀

▶

Back

Close

Full Screen / Esc

Printer-friendly Version

Interactive Discussion



$\beta_{p, //}(\lambda)$ and $\beta_{p, \perp}(\lambda)$ at wavelength λ_1 and λ_2 . In addition, accurate numerical simulations, to be addressed in Sect. 4, are needed to determine Eq. (15e, f) to (15l). In the literature, the spectral dependence of β_p is given in the form of the so-called Angstrom exponent \dot{A}_p which gives an indication on the particles size, as first shown by Sasano and Browell (1989). Note that the Angstrom exponent considered here differs from the traditional definition which specifies the wavelength dependence of the aerosol optical depth; both definitions indicate particle size, however. Hence, Eq. (15k) and (15l) can be rewritten as follows by introducing a cross-polarized ns-particle Angstrom exponent $\dot{A}_{ns, \perp}(\lambda_1, \lambda_2)$:

$$\left(\frac{\lambda_2}{\lambda_1}\right)^{-\dot{A}_{ns, \perp}} = \left\langle \left(\frac{d\sigma}{d\Omega} \right)_{ns, \perp}(\lambda_2) \right\rangle / \left\langle \left(\frac{d\sigma}{d\Omega} \right)_{ns, \perp}(\lambda_1) \right\rangle \quad (17)$$

where the equations holds for both ns1 and ns2-particles, so that equivalently, the ratio of cross-polarized backscattering cross-sections, which appears in Eq. (15k) and (15l), can be given in terms of the corresponding cross-polarized ns-particle Angstrom exponents $\dot{A}_{ns, \perp}(\lambda_1, \lambda_2)$. Hence, four Lidar-retrieved backscattering coefficients $\beta_{p, //}(\lambda), \beta_{p, \perp}(\lambda)$ with $\lambda = \{ \lambda_1, \lambda_2 \}$, addressed in Sect. 3, are used in combination with eight numerically-retrieved quantities $[\delta_{ns1}(\lambda), \delta_{ns2}(\lambda), \delta_{n12}(\lambda), \dot{A}_{ns1, \perp}(\lambda_1, \lambda_2), \dot{A}_{ns2, \perp}(\lambda_1, \lambda_2)]$, addressed in Sect. 4, to determine the twelve ns-particles backscattering coefficients $\beta_{p, \pi}(\lambda)$, with $(p) = \{ ns1, ns2, n12 \}$ and $\pi = \{ //, \perp \}$.

3 UV-VIS polarization Lidar remote sensing experiment

3.1 Lyon Lidar experimental set-up

Our dual-wavelength polarization Lidar experimental set-up has been extensively described in (David et al., 2012) where the design, the optimization and the performance of this home-built set-up are detailed. Lyon polarization Lidar is composed of a doubled

and tripled-Nd:YAG laser emitting 10 ns-laser pulses at 355 and 532 nm with 10 mJ of energy and a high degree of polarization (10 000 : 1). Backscattered photons are collected with an f/3-Newtonian telescope before entering a home-built polarization detector where they are (λ, π) -separated using dichroic mirrors and polarizing beam-splitter cubes (PBC). As shown in Fig. 2, each linear polarization channel has two PBC's to ensure an efficient partitioning between s and ns-particle backscattering, using state-of-the-art optical components in the UV and the VIS spectral ranges. To minimize any possible bias in the polarization measurement, we have quantitatively verified the specifications of each optical component at our laboratory on a dedicated test-bench. Polarization cross-talks, ensuring efficient s and ns-particles separation, are fully negligible with 10^{-7} accuracy. Particle depolarization ratio measurements as low as 6×10^{-3} , comparable to the molecular depolarization, have been achieved for tropospheric aerosol remote sensing, which are very low values for atmospheric lidar observations (David et al., 2012). Moreover, precise laboratory alignment ensures that the same atmospheric volume is probed in the UV and the VIS spectral ranges. Finally, interference filters are used to minimize sky background contribution as well as molecular backscattering, which is strong in the UV-spectral range. When exiting the photomultiplier tubes (PMT), the induced photoelectrons are sampled by a Licel TR-20 MHz, leading to 75 m-vertical range resolution after range-averaging.

3.2 Particle depolarization ratio and backscattering coefficient vertical profiles

To quantify the amount of ns-particles in the atmosphere, a precise polarization calibration of the detector is necessary, as detailed below. We applied the methodology proposed by Alvarez et al. (2006), which consists of applying controlled amounts of polarization cross-talks directed at studied altitudes. The detector gain electro-optics calibration constant is hence known with better than 2 % uncertainty (David et al., 2012), allowing accurate measurement of the depolarization ratio δ at wavelength λ . The depolarization ratio δ is not only due to atmospheric particles, but also due to atmospheric molecules, which strongly scatter light in the UV spectral range. Molecular anisotropy is

Retrieving volcanic, desert dust, and sea-salt particle properties

G. David et al.

Title Page

Abstract

Introduction

Conclusions

References

Tables

Figures



Back

Close

Full Screen / Esc

Printer-friendly Version

Interactive Discussion



responsible for the appearance of Raman rotational sidebands, leading to a molecular depolarization ratio $\delta_m = 3.7 \times 10^{-3}$, determined by applying optical molecular scattering theory for our interference filter bandwidth. The δ -ratio being non-additive, it is linked to the (size-averaged) particle depolarization ratio δ_p and molecular depolarization ratio δ_m through the contrast $R_{//} = 1 + \beta_{p, //} / \beta_{m, //}$ of molecular-to-particle backscattering, called the parallel Lidar R-ratio:

$$\delta(\lambda) = \left(1 - \frac{1}{R_{//}}\right) \delta_p(\lambda) + \frac{\delta_m}{R_{//}} \quad (18)$$

Hence, a particle-free or molecular atmosphere corresponds to $R_{//} = 1$. We computed $R_{//}$ by applying the Klett's algorithm to the parallel Lidar channel to correct for the particle extinction, using an extinction-to-backscatter S_p -ratio, derived from numerical simulations to be detailed in Sect. 4. In this paper, we focus on the mixing of particles in the free troposphere, for altitudes above $z = 1.2$ km above mean sea level. At lower altitudes, the particle load is dominated by local aerosols, and a complex mixture of soot, aggregated and local pollutants, is present, as discussed by Miffre et al. (2010). The Klett inversion must then account for the effects of moisture, so that a more complex S_p -computation is needed David et al. (2012). The accuracy on the parallel Lidar ratio is derived from the Klett's algorithm, using the maximum and minimum values of S_p . Then, using reanalysis model from the European Centre for Medium-range Weather Forecasts (ECMWF), we derived the $\beta_{m, //}$ -vertical profile to retrieve the co-polarized particle backscattering coefficient as a function of z -altitude:

$$\beta_{p, //}(\lambda) = (R_{//} - 1) \times \beta_{m, //} \quad (19)$$

The cross-polarized particle backscattering coefficient $\beta_{p, \perp}(\lambda)$, which is specific to non-spherical particles, is then derived from $R_{//}$ and δ by using Eq. (19) and the δ_p -definition ($\delta_p = \beta_{p, \perp} / \beta_{p, //}$):

$$\beta_{p, \perp}(\lambda) = (R_{//} \delta - \delta_m) \times \beta_{m, //} \quad (20)$$

Retrieving volcanic, desert dust, and sea-salt particle properties

G. David et al.

Title Page

Abstract

Introduction

Conclusions

References

Tables

Figures

◀

▶

◀

▶

Back

Close

Full Screen / Esc

Printer-friendly Version

Interactive Discussion



Finally, the particle depolarization ratio δ_p is derived from Winker and Osborn's procedure (1992) using $R_{//}$ and δ :

$$\delta_p(\lambda) = (R_{//}\delta - \delta_m)/(R_{//} - 1) \quad (21)$$

At an altitude z , error bars on δ_p are calculated by using Eq. (21). The uncertainty on δ_p originates from the $R_{//}$ -uncertainty, determined by the S_p -uncertainty, and from the δ -ratio uncertainty, derived from the measured polarization Lidar signals after accurate calibration. To reduce statistical errors, each vertical profile is an average from 4000 lasers shots.

4 Numerical experiments on nonspherical particles

As explained in Sect. 2, a polarization-resolved Lidar experiment is sensitive to both s and ns-particles in the particle mixture. The purpose of this section is to derive the optical backscattering and depolarization properties of ns-particles from a three-component mixture. We here compute the necessary lidar scattering properties for the ns-particles ensemble by using single-scattering models. Since the century-old Lorentz-Mie theory does not apply to ns-particles, which scatter light differently from volume or surface-equivalent spheres (Nousiainen, 2009), we have applied the T-matrix algorithm (Mishchenko et al., 1998) to compute the ns-particle scattering matrix elements for volcanic ash and desert dust particles in our controlled numerical experiments. For sea salt, we have used the T-matrix algorithm by Kahnert (2013). In the T-matrix method, an exact solution derived from the Maxwell's equations can be obtained, with an analytical orientation averaging, when the ns-particle shapes are sufficiently simple. In this section, a one-component atmosphere is assumed, i.e. numerical simulations are relative to one ns-particle component, either ash, dust or sea-salt particles. Backscattering cross-sections β_{ns} , depolarization ratios δ_{ns} and extinction-to-backscatter ratios S_{ns} are numerically computed for these ns-particles. The δ_{ns} -values

Retrieving volcanic, desert dust, and sea-salt particle properties

G. David et al.

Title Page

Abstract

Introduction

Conclusions

References

Tables

Figures

⏪

⏩

◀

▶

Back

Close

Full Screen / Esc

Printer-friendly Version

Interactive Discussion



are then discussed in the UV and the VIS spectral ranges. Moreover, the spectral behavior of the backscattering coefficient β_{ns} is retrieved for each ns-particle type (ash, dust, sea-salt) present in the particle mixture.

4.1 Methodology

5 The optical properties of volcanic ash, desert dust or sea-salt particles encountered in the atmosphere are difficult to simulate with numerical models, due to the strong complexity of these highly-irregularly shaped ns-particles. As underlined in (Nousiainen (2009) and Nousiainen et al. (2012), a complete realistic modelling should account for the ns-particles' inhomogeneity, aggregation, morphological effects, as well as possible porosity or birefringence. Despite the complexity, it is now well-established that the optical properties of size-shape distributions of such particles can be well-mimicked by size-shape distributions of homogeneous spheroids, at least when particles are not much bigger than the wavelength. The shapes of spheroids are expressed by the so-called aspect ratio $\varepsilon = b/a$, where a and b are the major and minor axis lengths, respectively. The orientation and shape averaging, which smooth out the scattering matrix elements, probably plays a role in the ability of the homogeneous spheroid model to mimic optical properties encountered in the atmosphere (Nousiainen et al., 2012). For example, Nousiainen and Vermeulen (2003), Nousiainen et al. (2006), Dubovik et al. (2006) as well as Veselovskii et al. (2010) and Merikallio et al. (2011) have demonstrated that a mixture of randomly-oriented spheroids with different sizes and aspect ratios can reproduce the phase function for dust particles. Other approaches, such as the DDA-method (Draine and Flatau, 1994), are also feasible and promising but clearly beyond the scope of this paper, aimed at presenting a possible modelling of atmospheric ns-particles to be applied to polarization Lidar measurements in Sect. 5, using the Sect. 2-developed methodology.

25 We have performed numerical T-matrix computations (Mishchenko et al., 1998 for spheroids, Kahnert, 2013 for cubes) for volcanic ash, desert dust and sea-salt particles to compute their scattering matrix $[\mathbf{F}]_{\text{ns}}$ as a function of the size parameter x at the

Retrieving volcanic, desert dust, and sea-salt particle properties

G. David et al.

Title Page

Abstract

Introduction

Conclusions

References

Tables

Figures

⏪

⏩

◀

▶

Back

Close

Full Screen / Esc

Printer-friendly Version

Interactive Discussion



Retrieving volcanic, desert dust, and sea-salt particle properties

G. David et al.

Title Page

Abstract

Introduction

Conclusions

References

Tables

Figures

⏪

⏩

◀

▶

Back

Close

Full Screen / Esc

Printer-friendly Version

Interactive Discussion

Lidar backscattering angle. The algorithm also calculates the scattering cross-section $C_{\text{sca,ns}}$ and extinction $C_{\text{ext,ns}}$ as a function of the particle radius and radiation wavelength λ . We assume the ns-particle ensemble to be composed of randomly oriented 50% oblate ($\varepsilon \geq 1$) and 50% prolate ($\varepsilon < 1$) spheroid particles, used as a proxy to represent atmospheric ns-particles. A natural basic assumption would be to consider that all spheroids have equal number concentrations (equi-probable shape distribution). However, as described in (Merikallio et al., 2011), atmospheric samples measured in laboratory measurements (Volten et al., 2001; Muñoz et al., 2004) are more realistically mimicked by a power-law $n = 3$ shape distribution. This favours extreme aspect ratio at the expense of nearly spherical spheroids, but in this way, polarization effects are better taken into account. The size parameters were chosen to be representative of atmospheric ns-particles after long-range transport. As detailed in (Schumann et al., 2011), sedimentation effects may modify the ns-particles' size distribution. Moreover, in the case of a sea-salt and dust particle mixture, sea-salt adhering may cause the gravitational settling of dust particles to be significantly accelerated (Zhang, 2008). Thus, for a given travel distance, a cut-off radius of a few micrometers seems reasonable according to the literature. Accordingly, we chose x-values varying from 0.01 to 50 after long-range transport and ran the T-matrix code for volcanic ash and desert dust particles, using the m-refractive indices given in Table 2, for eight ε -bins, varying from 1.2 up to 2.6. As described in Sect. 2.1, sea-salt particles often exhibit a cube-like shape. Hence, to compute the optical properties of sea-salt particles, we applied an extension of the T-matrix code developed by M. Kahnert (2013). This code, which exploits the group theory to efficiently compute different targets with discrete symmetries, is well-suited to compute the optical properties of particles having discrete symmetries such as polyhedral prisms or cubes. Table 2 summarizes the input parameters used in the simulations for each particle component: ash, dust, sea-salt particles.

4.2 Backscattering and depolarization of light by a single ns-particle

We have computed $F_{11,ns}$, $F_{22,ns}$, $C_{sca,ns}$ and $C_{ext,ns}$ as a function of the particle radius r for ash, dust, sea-salt and water-soluble particles at the $\lambda_1 = 355$ nm and $\lambda_2 = 532$ nm Lidar wavelengths at the Lidar backscattering angle. Using Eqs. (3), (7), we display in Fig. 3 the particle backscattering cross-sections $(d\sigma/d\Omega)_{p, //}$ and $(d\sigma/d\Omega)_{p, \perp}$ and the ns-particle depolarization ratio δ_{ns} as a function of the particles radius r . For clarity, the backscattering cross-sections are plotted per unit volume to emphasize the role of wavelength-sized particles, as first done in (Veselovskii et al., 2010). The obtained curves agree with the literature on spheroid particles (Veselovskii et al., 2010; Mishchenko et al., 2009). In particular, the backscattering cross-sections are not monotonic with the particle radius r . Due to the homothetic scale in r/λ , wavelength-sized particles exhibit larger backscattering cross-sections in the UV spectral range at $\lambda_1 = 355$ nm than in the VIS spectral range at $\lambda_2 = 532$ nm. Hence, our sensitivity to the fine particles mode (particles having a radius in the range of 100 nm) is increased in the UV. As expected, s-particles do not depolarize laser light at the Lidar backscattering angle. The ns-particles' depolarization ratio reaches its maximum value around $r = 0.3 \mu\text{m}$ in the UV ($0.5 \mu\text{m}$ in the VIS). Above this maximum, the dependence of δ_{ns} with r exhibits weak secondary maxima, but is otherwise almost constant when increasing the particles radius. Below $r = 0.5 \mu\text{m}$, δ_{ns} rapidly increases with r and depolarization ratios as high as 50 % are reached so that ns-particles in the fine mode may also depolarize laser light. This result should be taken into account in recent field studies (Ansmann et al., 2012). Such high depolarization ratios may be experimentally observed with a Lidar as long as these ns-particles are mainly contributing to ns-particle backscattering. Hence, nano-sized ns-particles depolarize laser light as recently demonstrated in Dupart et al. (2012). However, δ_{ns} cannot be used as a particle size-meter since it also depends on m and ε (Mishchenko et al., 1995).

Retrieving volcanic, desert dust, and sea-salt particle properties

G. David et al.

Title Page

Abstract

Introduction

Conclusions

References

Tables

Figures

⏪

⏩

◀

▶

Back

Close

Full Screen / Esc

Printer-friendly Version

Interactive Discussion



4.3 Backscattering and depolarization of light by an ensemble of ns-particles

In lidar applications, the optical properties are integrated over the particle sizes and shapes. Ideally, the ns-particles size distribution (PSD) should hence be accurately measured. In the absence of complementary measurements, the ns-PSD has been taken from the literature on atmospheric ns-particles after long-range transport, with the criteria of ensuring ns-particle specificity since our numerical simulations are built for that purpose. As an example, Muñoz et al.'s (2004) PSD was chosen for volcanic ash particles, since it is by construction ash-particles specific, while being representative of long-range transport since samples were mechanically sieved to remove the largest particles, as for gravitational settling. Hence, this PSD is representative of volcanic ash after long-range transport, as detailed in Miffre et al. (2012b). The chosen ns-PSD are displayed in Fig. 4, for the ns-particle types considered.

As described in Eq. (4), integration of $(d\sigma/d\Omega)_{ns, //}$, $(d\sigma/d\Omega)_{ns, \perp}$ over the PSD leads to the β_{ns} -coefficient plotted in Fig. 5 as a function of the wavelength. For volcanic ash and desert dust particles, with this choice of PSD, the $\beta_{ns, \perp}$ -coefficient is higher in the UV spectral range than in the VIS-spectral range, while an opposite behavior is observed for sea-salt particles. The wavelength-dependence of δ_{ns} is also displayed. The observed dependence agrees with the literature as for desert dust particles for example (Veselovskii et al., 2010). However, the ash particle depolarization δ_{ash} is different from those found in the literature (Muñoz et al., 2004; Lindqvist et al., 2011). The discrepancy may originate from surface roughness, which is more important for larger particles and is not accounted for in our spheroid model: the Fig. 3 tendency of δ_{ns} to be constant while increasing effective radius is not observed in laboratory measurements where δ_{ns} tends to increase with increasing particle radius (Nousiainen, 2009). It follows that spheroids may have difficulties in predicting large particle depolarization ratios such as for volcanic ash correctly. Hence, for volcanic ash, we may use O. Muñoz's laboratory measurements $\delta_{ash} = 40.5\%$ -value (2004), leaving more appropriate δ_{ash} -numerical simulations for a forthcoming paper. Finally, using Eq. (6), we computed the

Retrieving volcanic, desert dust, and sea-salt particle properties

G. David et al.

[Title Page](#)[Abstract](#)[Introduction](#)[Conclusions](#)[References](#)[Tables](#)[Figures](#)[⏪](#)[⏩](#)[◀](#)[▶](#)[Back](#)[Close](#)[Full Screen / Esc](#)[Printer-friendly Version](#)[Interactive Discussion](#)

extinction-to-backscatter ratio S_{ns} in Fig. 5 as a function of wavelength. The obtained S_{ns} -value agrees with the literature, derived from Raman Lidar measurements. For example, at $\lambda_1 = 355$ nm, S_{ash} equals (60 ± 5) sr at Munich (Ansmann et al., 2012), while for dust particles, Veselovskii et al. (2010) numerically computed $S_{dust} = 68$ sr. Sea-salt particles exhibit S_{ns} -values around 20 sr, in agreement with (Ansmann et al., 2011).

4.4 Summary of the numerical simulations on ns-particles

Table 3 summarizes the results of our T-matrix simulations to be used in Sect. 5 for ns-particles: the depolarization ratio δ_{ns} averaged over the corresponding PSD is given at the two Lidar wavelengths, together with the cross-polarized Angstrom exponent $\dot{A}_{ns,\perp}(\lambda_1 = 355$ nm, $\lambda_2 = 532$ nm) and the extinction-to-backscatter ratio S_{ns} needed for the Klett inversion. The sign of $\dot{A}_{ns,\perp}$ (UV, VIS) underlines our chosen PSD: dust (resp. sea-salt) particles backscatter more light in the UV (resp. VIS) spectral range than in the VIS (resp. UV) spectral range.

5 Application to volcanic ash, desert dust and sea-salt particle mixing

In this section, the composition of the particles' external mixture is analyzed experimentally after long-range transport through 2λ -polarization-resolved backscattering measurements performed at Lyon, France. Taking advantage of the sensitivity and accuracy achieved in the UV-VIS polarization Lidar experiment and the numerical simulations carried out, the backscattering coefficients specific to volcanic ash, desert dust and sea-salt particles are retrieved by applying the methodology developed in Sect. 2, in two studied cases:

Case 1 is an example of depolarization of light by a two-component particle mixture after long-range transport. During the 2010 Eyjafjallajökull volcanic eruption, large quantities of volcanic ash was injected into the troposphere, leading to a safety related six-day airport closure. After more than 2500 km of transport by advection, the

Retrieving volcanic, desert dust, and sea-salt particle properties

G. David et al.

Title Page

Abstract

Introduction

Conclusions

References

Tables

Figures

⏪

⏩

◀

▶

Back

Close

Full Screen / Esc

Printer-friendly Version

Interactive Discussion

volcanic ash particles entering Lyon's atmosphere were mixed with spherical particles, most likely to be hydrated sulphates, produced by SO₂-oxydation (Mather et al., 2003), giving rise to a two-component external mixture.

Case 2 is an example of depolarization of light by a three-component particle mixture after long-range transport. On 18 October 2011, a Saharan dust outbreak occurred at Lyon with particles entering the Lyon troposphere after several thousand kilometres of transport by advection above the Atlantic Ocean, during which they mixed with sea-salt particles and in the troposphere over Lyon with local aerosols. This { desert dust, sea-salt, water-soluble} particle mixture is an example of a three-component external mixture.

5.1 Case study 1: mixing of Eyjafjallajökull volcanic dust with sulfate particles

As shown by FLEXPART ash particle numerical dispersion model and 7-days air mass back-trajectories (see Fig. 7), volcanic ash particles released from the Eyjafjallajökull volcano passed above Lyon on 19 April 2010 around 19:00 UTC above 3 km altitude above mean sea level. Using the methodology introduced in Sect. 3.2, we display in Fig. 7 vertical profiles of atmospheric particle UV-backscattering coefficients $\beta_{p, //}$, $\beta_{p, \perp}$ and particle depolarization ratio δ_p on 19 April 2010 at 19:00 UTC, using $S = 55 \pm 5$ sr for the Klett algorithm. As a consequence of Eq. (10), the co- and cross-polarized backscattering coefficients plotted in Fig. 8 are different. The presence of s-particles lowers the observed δ_p -values, which are always below δ_{ash} within our error bars. It follows that, contrary to what is generally observed in the literature, the maximum observed δ_p -value cannot be taken as a δ_{ns} -measurement.

Contrary to the δ_p -profile, only ash particles contribute to the $\beta_{p, \perp}$ -vertical profile, as discussed in Sect. 2.3. Thus, the vertical dispersion of the volcanic ash cloud in the low troposphere of Lyon can be retraced by the $\beta_{p, \perp}$ -vertical profile: within our error bars, the achieved sensitivity allows distinguishing several successive volcanic ash layers at about 1.5, 2.5, 3.5, 4.7 km altitudes. This result is best seen on the observed β_{ash} -vertical profile, using Eq. (14) with $\delta_{ash} = 40.5\%$ (Muñoz et al., 2004) and

Retrieving volcanic, desert dust, and sea-salt particle properties

G. David et al.

Title Page

Abstract

Introduction

Conclusions

References

Tables

Figures

⏪

⏩

◀

▶

Back

Close

Full Screen / Esc

Printer-friendly Version

Interactive Discussion



$\delta_{\text{non-ash}} = 1\%$ (Sakai et al., 2010). As shown by the comparison of the $\beta_{p,\perp}$ and δ_p -vertical profiles, depolarization does not necessarily correlate with the backscattered power. The observed 3.5-km altitude difference between the $\beta_{p,\perp}$ and the δ_p -maxima is due to the presence of spherical sulphate particles, produced by SO_2 -oxydation after long-range transport. The similarity between the X_{ash} -profile and the δ_p -profile shows that δ_p can be considered in our case as a tracer for X_{ash} in agreement with Eq. (13). In the literature, δ_p is sometimes considered as a tracer for ash particles, which is true when backscattering is strongly dominated by ash, close to the source region (Gasteiger et al., 2011). Here, our long-range transport situation implies that s-particles are present in significant numbers, so that $\beta_{p,\perp}$ is a tracer for the volcanic ash particles. From the ash and sulphate backscattering coefficients, number concentrations can be retrieved, and the values obtained agree with those measured by Schumann et al. (2011). This application is however beyond the scope of this paper and has already been published elsewhere, by also taking into account the possible influence of sedimentation effects on the retrieved ash particles number concentration (Miffre et al., 2012b), then further transformed into ash mass concentrations (Miffre et al., 2012a). Use of Schumann et al.'s (2011) PSD instead of Muñoz et al.'s PSD (2004) led to only 3% lower ash number concentration, which shows the robustness of our methodology. In addition, case study 1 can be extended to a two-component particles mixture composed of dust and spherical particles, as published in Miffre et al. (2011).

5.2 Case study 2: mixing of desert dust, sea-salt and water-soluble particles

The second case study is related to the mixing of desert dust particles with sea-salt and water soluble particles after long-range transport. Such a particle mixture occurred at Lyon for example on 18 October 2011 due to favourable meteorological conditions after more than 2500 km advection from the dust source region.

Retrieving volcanic, desert dust, and sea-salt particle properties

G. David et al.

[Title Page](#)[Abstract](#)[Introduction](#)[Conclusions](#)[References](#)[Tables](#)[Figures](#)[⏪](#)[⏩](#)[◀](#)[▶](#)[Back](#)[Close](#)[Full Screen / Esc](#)[Printer-friendly Version](#)[Interactive Discussion](#)

5.2.1 Meteorological and geophysical situation

As shown by FLEXTRA 7-days air mass back-trajectories (see Fig. 8), in the morning of 18 October 2011, sea-salt particles were present at Lyon about 1.5 km altitude (*a*-layer) while desert dust particles were located around 3 km (*b*-layer). In the evening, sea-salt particles were present around the *b*-layer, while desert dust particles were mostly detected in the *a*-layer. Hence, a mixing of sea-salt and desert dust particles occurred during daytime in the low troposphere. The *a*- and *b*-layers are delimited by temperature inversion layers that can be seen in the vertical profiles of potential temperature, also present in Fig. 8, showing that the troposphere was stably stratified. For altitudes above 2 km, the relative humidity (RH) was above 40 %, corresponding to the sodium chloride crystallization point. Hence, at these altitudes, the cubic shape model was applicable for sea-salt particles, in agreement with Sect. 2.1.

5.2.2 Separate retrieval of vertical profiles of atmospheric dust, sea-salt and water-soluble particles

By performing sensitive and accurate UV-VIS polarization Lidar measurements, using the Sect. 3.2 methodology, we derived time-altitude maps of co-, cross-polarized backscattering coefficients and particle depolarization ratio δ_p as displayed in Fig. 9. To correct for the particle extinction, we chose $S(UV) = 50 \pm 5$ sr and $S(VIS) = 60 \pm 5$ sr, in agreement with the literature (Murayama et al., 1999). These values are between computed values for S_{dust} and S_{ss} . Each time-altitude map has adjusted colour scales to emphasize the achieved sensitivity that clearly brings out the temporal behavior of two main atmospheric layers having different thicknesses, located around the *a*- and the *b*-layers. This layering is clearly visible in the UV and VIS cross-polarized backscattering time-altitude maps, which are ns-particles specific, as shown by Eq. (10-b). In agreement with Sect. 2.3.1, the particle depolarization ratio maps exhibit maximum δ_p -values equal to 11 % at $\lambda_1 = 355$ nm and 9 % at $\lambda_2 = 532$ nm, well below the δ_{ns} -values computed for sea-salt or dust particles (see Table 3). By combining the light scattering

Retrieving volcanic, desert dust, and sea-salt particle properties

G. David et al.

Title Page

Abstract

Introduction

Conclusions

References

Tables

Figures

⏪

⏩

◀

▶

Back

Close

Full Screen / Esc

Printer-friendly Version

Interactive Discussion



simulations presented in Sect. 4 with our UV-VIS polarization measurements, we have run our $2\beta + 2\delta$ algorithm to solve the set of 12 Eq. (15) and separately retrieve the backscattering coefficients of desert dust, sea-salt (ss) and water soluble (ws) particles as a function of altitude on 18 October 2011 at 16:15 UTC (see Fig. 9 vertical dashed-lines). Figure 10 displays the retrieved vertical profiles of β_{dust} , β_{ss} and β_{ws} , together with the corresponding $\beta_{\text{p},//}$, $\beta_{\text{p},\perp}$ and δ_{p} vertical profiles and the fraction of each component (dust, ss, ws) in the mixed particles cloud at 16:15 UTC. For the first time, the nonsphericity of both dust and sea-salt particles is taken into account, which is essential since RH-values are well below the 40 % relative humidity sea-salt crystallization point, allowing sea salt particles to depolarize.

5.2.3 Discussion on the retrieved vertical profiles of atmospheric dust, sea-salt and water-soluble particles

The retrieved vertical profiles of atmospheric dust, sea-salt and ws-particle backscattering have been obtained by combining sensitive and accurate UV-VIS polarization Lidar measurements with accurate T-matrix numerical simulations. As a stand-alone Lidar experiment provides no chemical analysis, 7-days air mass back-trajectories have been used to address the ns-particles type. Finally, the RH-vertical profile has been a useful tool to check the consistency of the cubic shape approximation for ss-particles. This methodology is complex, but it is a necessity for particle mixtures observation after long-range transport where the approximation $\delta_{\text{p}} = \delta_{\text{ns}}$ no longer holds. This methodology, because it is new, is yet to be validated in the atmosphere. Such a validation work is now under progress and will be the subject of a forthcoming paper. We here discuss the possible influence of computed numerical values of δ_{ns} and $\dot{A}_{\text{ns},\perp}$ (UV, VIS) for dust and ss-particles (see Table 3 for the used numerical values) on the retrieval results. To test the robustness of our new methodology, we used exaggerated δ_{ss} and $\dot{A}_{\text{ns},\perp}$ (UV, VIS) values. As shown by Eq. (11), the effect of a different δ_{ns} -value is to shift the corresponding β_{ns} -vertical profile. Hence, the behavior of β_{ns} with altitude is still retraced for a different δ_{ns} -value. To be quantitative, when using $\delta_{\text{ss}} = 33\%$ instead of 10 %, 1922

Retrieving volcanic, desert dust, and sea-salt particle properties

G. David et al.

[Title Page](#)[Abstract](#)[Introduction](#)[Conclusions](#)[References](#)[Tables](#)[Figures](#)[⏪](#)[⏩](#)[◀](#)[▶](#)[Back](#)[Close](#)[Full Screen / Esc](#)[Printer-friendly Version](#)[Interactive Discussion](#)

Retrieving volcanic, desert dust, and sea-salt particle properties

G. David et al.

Title Page

Abstract

Introduction

Conclusions

References

Tables

Figures

⏪

⏩

◀

▶

Back

Close

Full Screen / Esc

Printer-friendly Version

Interactive Discussion

β_{ss} decreases by a factor of almost 3 (11/4 exactly), which in turn may increase the observed β_{ws} -value, depending on the observed corresponding β_{dust} -value. Assuming that sea-salt particles do not depolarize laser light ($\delta_{ss} = 0$) was not easily feasible, due to the singularity hence introduced in Eq. (11). However, very close to $\delta_{ss} = 0$, we noticed that the retrieved β_{ss} and β_{ws} -values were very different from those observed in Fig. 10, hence underlying the importance of taking into account the ss-particle nonsphericity when RH-values allow ss-particles to be nonspherical. The computed cross-polarized Angstrom exponent $\dot{A}_{ns,\perp}$ (UV, VIS) may also be questioned. In agreement with Sect. 4, Fig. 10 shows that dust particles contribute more to particle backscattering at the UV spectral range than in the VIS, while sea salt-particle backscattering is stronger in the VIS spectral range. The $\dot{A}_{dust,\perp}$ (UV, VIS) and $\dot{A}_{ss,\perp}$ (UV, VIS) values can be considered as convergence criteria in our algorithm, since for very different values of $\dot{A}_{dust,\perp}$ (UV, VIS) and $\dot{A}_{ss,\perp}$ (UV, VIS), negative particle backscattering coefficients were retrieved. Hence, to obtain accurate retrievals of dust, sea-salt and ws-particles backscattering coefficients, care should be taken on the choice of PSD when applying our new methodology. Moreover, by using UV-VIS laser light, we have increased our sensitivity to particles in the fine and coarse particles mode. Hence, precise polarization measurement allows minimizing the contribution of possible frozen hydrometeors which may be present in the troposphere.

The vertical profiles of dust, sea-salt and ws-particles plotted in Fig. 10 thus reveal a complex vertical layering of the Lyon troposphere. In contrast to what is observed with a two-component mixture, due to the ws-particles presence, the β_{dust} -vertical profile is not complementary of the β_{ss} -vertical profile. We here analyze the obtained vertical profiles in the *a*- and the *b*-layers. Up to 3.0 km altitude, where a temperature inversion is observed, in the *a*-layer, dust (resp. sea-salt) particles contribute to nearly 40% (resp. 10%) to the total particle backscattering coefficient. The vertical profile of ws-particles is much more complicated to describe, except when X_{ss} is constant such as between 2.7 and 3.0 km altitude, in which case X_{dust} and X_{ws} are in opposite phases with respect to altitude. Despite its complex behavior, the β_{ws} -vertical profile nearly

follows the $\beta_{p, //}$ -vertical profile, for which s-particles mainly contribute. Above 3.0 km altitude, in the *b*-layer, the fractions of dust, ss and ws-particles in the total particle backscattering vary with altitude: a very complex vertical layering is hence revealed. A very interesting point is to be seen around the extrema observed at a 3.5 km altitude where, in the UV, the β_{dust} and the β_{ws} -vertical profiles are in opposite phases with respect to altitude. As recently shown in Dupart et al. (2012), this behavior can be related to new particles formation events. This observation clearly indicates that the proposed methodology is able to reveal very complex particles microphysical behavior, which in turn favours the proposed methodology.

6 Conclusions and outlook

In this contribution, the depolarization of light by atmospheric nonspherical particles has been used to evaluate the partitioning of a two or a three-component particle external mixtures of volcanic ash, desert dust, sea-salt and water-soluble particles. This partitioning is particularly interesting after long-range transport, where the mixing of these particles is often observed. In Sect. 2, where our methodology is described in detail, we showed that, after long-range transport, the depolarization δ_p of the particle mixture differs from the depolarization δ_{ns} of its ns-particles, as a consequence of the presence of s-particles, which contribute to δ_p . Hence, and as a first result, care should be taken when using the maximum value of δ_p as a proxy for δ_{ns} . This assumption, which is often done in the literature, may be false after long-range transport where s-particles are present and contribute to δ_p . We thus developed a new methodology to retrieve separate vertical profiles for atmospheric volcanic ash, dust, sea-salt particles in two/three component particle external mixtures. This methodology relies on the combined use of a 2λ -polarization Lidar and accurate T-matrix numerical simulations, used for computing the backscattering (β_{ns}) and depolarization properties (δ_{ns}) of each nonspherical particle type (ash, dust, sea-salt) present in the two/three component external mixture. In addition, air mass back-trajectories are needed to identify

Retrieving volcanic, desert dust, and sea-salt particle properties

G. David et al.

[Title Page](#)[Abstract](#)[Introduction](#)[Conclusions](#)[References](#)[Tables](#)[Figures](#)[⏪](#)[⏩](#)[◀](#)[▶](#)[Back](#)[Close](#)[Full Screen / Esc](#)[Printer-friendly Version](#)[Interactive Discussion](#)

**Retrieving volcanic,
desert dust, and
sea-salt particle
properties**

G. David et al.

Title Page

Abstract

Introduction

Conclusions

References

Tables

Figures

⏪

⏩

◀

▶

Back

Close

Full Screen / Esc

Printer-friendly Version

Interactive Discussion



the ns-particle type present at the remote site. The originality of this work precisely consists in combining instruments (polarization Lidar, T-matrix simulations) that are often used separately in the literature, where measured δ_p -values are often compared to computed δ_{ns} -values. Using our sensitive and accurate UV-VIS polarization Lidar experiment (see Sect. 3), we hence retrieved vertical profiles of atmospheric volcanic dust mixed with spherical sulphate (case 1), before studying the mixing of desert dust particles with sea-salt and water-soluble particles (case 2) by using our newly developed $2\beta + 2\delta$ -algorithm. We used both spectral (λ) and polarization (π) properties of the light backscattered by atmospheric ns-particles. To our knowledge for the first time, a three-component external mixture has been partitioned into its ns-particles components by taking into account the nonsphericity of each ns-particles component (i.e. in the proposed case study 2, sea-salt and dust particles nonsphericity). The assumption of sea-salt particle nonsphericity appeared prudent after carefully looking at the RH-vertical profiles during the analyzed Saharan dust outbreak. Thanks to our achieved sensitivity and accuracy on our UV-VIS polarization Lidar experiment, the complex vertical layering of the Lyon troposphere was clearly seen by applying this new methodology, which exhibits separate contributions of dust, sea-salt and water-soluble particles in the particle mixture. The robustness of the proposed methodology has also been studied by running the $2\beta + 2\delta$ -algorithm using out-of-range values for the dust and sea-salt particles depolarization ratio. It should be noted that, to apply this new methodology, care should be taken with the ns-particle size distribution assumed in the numerical computations, which must be ns-particle specific and representative of these ns-particles after long-range transport. A further validation of this methodology is clearly needed and will be published in the next paper. Moreover, the methodology could be further improved. To quote only a few possible steps, for the numerical simulations, an extension to some more complex and realistic shapes using DDA-approximation (Noussiainen et al., 2012) or/and including porosity effects (Lindqvist et al., 2012) would be desirable. For the polarization Lidar experiment, as underlined by Nicolet et al. (2012), use of circular depolarization might also provide new insights. To conclude, we showed

that the combined use of UV-VIS polarization Lidar remote sensing experiments with numerical simulations on ns-particles and air mass back-trajectories makes possible a range-resolved and robust analysis of atmospheric aerosols, up to three-component particle mixtures.

5 *Acknowledgements.* The authors thank M. Kahnert and M.I. Mishchenko for making their T-matrix codes available, O. Muñoz for proving the volcanic ash electron microscope image, A.M. Fjaeraa and A. Stohl from NILU for providing FLEXTRA air mass back-trajectories and FLEXPART ash numerical dispersion at Lyon, the Lyon Centre Technologie Microstructures for the use of the electron microscope and Région Rhône-Alpes for financial grant. In part, this
10 study has been funded by the Academy of Finland (contract 125180).

References

- Alvarez, J. M., Vaughan, M. A., Hostelier, C. A., Hunt, W. H., and Winker, D. M.: Calibration technique for polarization-sensitive Lidars, *J. Atmos. Ocean. Tech.*, 23, 683–699, 2006.
- 15 Ansmann, A., Petzold, A., Kandler, K., Tegen, I., Wendisch, M., Müller, D., Weinzierl, B., Müller, T., and Heintzenberg, J.: Saharan mineral dust experiments SAMUM–1 and SAMUM–2: what have we learned ?, *Tellus B*, 63, 403–429, 2011.
- Ansmann, A., Seifert, P., Tesche, M., and Wandinger, U.: Profiling of fine and coarse particle mass: case studies of Saharan dust and Eyjafjallajökull/Grimsvötn volcanic plumes, *Atmos. Chem. Phys.*, 12, 9399–9415, doi:10.5194/acp-12-9399-2012, 2012.
- 20 Baumgardner, D., Newton, R., and Boyouk, N.: The Aerosol Particle Spectrometer with Polarization Detection (APSPD) – Part I: Laboratory studies, *Atmos. Chem. Phys.*, in preparation, 2012.
- Bourcier, L., Sellegri, K., Chausse, P., Pichon, J. M., and Laj, P.: Seasonal variation of water-soluble inorganic components in aerosol size-segregated at the puy de Dome station (1465 m a.s.l.), France, *J. Atmos. Chem.*, 69, 47–66, 2011.
- 25 Boyouk, N., Léon, F. F., Delbarre, H., Podvin, T., and Deroo, C.: Impact of the mixing boundary layer on the relationship between $PM_{2.5}$ and aerosol optical thickness, *Atmos. Environ.*, 44, 271–277, 2010.

Retrieving volcanic, desert dust, and sea-salt particle properties

G. David et al.

Title Page

Abstract

Introduction

Conclusions

References

Tables

Figures

⏪

⏩

◀

▶

Back

Close

Full Screen / Esc

Printer-friendly Version

Interactive Discussion



Retrieving volcanic, desert dust, and sea-salt particle properties

G. David et al.

Title Page

Abstract

Introduction

Conclusions

References

Tables

Figures

⏪

⏩

◀

▶

Back

Close

Full Screen / Esc

Printer-friendly Version

Interactive Discussion



Córdoba-Jabonero, C., Guerrero-Rascado, J. L., Toledo, D., Parrondo, M., Yela, M., Gil, M., and Ochoa, H. A.: Depolarization ratio of Polar Stratospheric Clouds in coastal Antarctica: profiling comparison analysis between a ground-based Micro Pulse Lidar and the spaceborne CALIOP, *Atmos. Meas. Tech. Discuss.*, 5, 8051–8084, doi:10.5194/amtd-5-8051-2012, 2012.

David, G., Miffre, A., Thomas, B., and Rairoux, P.: Sensitive and accurate dual-wavelength UV-VIS polarization detector for optical remote sensing of tropospheric aerosols, *Appl. Phys. B*, 108, 197–216, 2012.

Di Girolamo, P., Summa, D., Bhawar, R., Di Iorio, T., Cacciani, M., Veselovskii, I., Dubovik, O., and Kolgotin A.: Raman lidar observations of a Saharan dust outbreak event: characterization of the dust optical properties and determination of particle size and microphysical parameters, *Atmos. Environ.*, 50, 66–78, 2012.

Draine, B. T. and Flatau, P. J.: Discrete-dipole approximation for scattering calculations, *J. Opt. Soc. Am.*, 11, 1491–1499, 1994.

Dubovik, O., Sinyuk, A., Lapyonok, T., Holben, B. N., Mishchenko, M., Yang, P., Eck, T. F., Volten H., Muñoz, O., Veihelmann, B., van der Zande, W. J., Leon, J.-F., Sorokin, M., and Slutsker, I.: Application of spheroid models to account for aerosol particle nonsphericity in remote sensing of desert dust, *J. Geophys. Res.*, 111, D11208, doi:10.1029/2005JD006619, 2006.

Dupart, Y., King, S. M., Nekat, B., Nowak, A., Wiedensohler, A., Herrmann, H., David, G., Thomas, B., Miffre, A., Rairoux, P., D'Anna, B., and George, C.: Mineral dust photochemistry induces nucleation events in the presence of SO₂, *Proc. Nat. Acad. Sci. USA*, 109, 20842–20847, doi:10.1073/pnas.1212297109, 2012.

Ehret, G., Kiemle, C., Wirth, M., Amediek, A., Fix, A., and Houweling S.: Space-borne remote sensing of CO₂, CH₄, and N₂O by integrated path differential absorption lidar: a sensitivity analysis, *Appl. Phys. B*, 90, 593–608, 2008.

Freudenthaler, V., Esselborn, M., Wiegner, M., Heese, B., Tesche, M., Ansmann, A., Müller, D., Althausen, D., Wirth, M., Fix, A., Ehret, G., Knippertz, P., Toledano, C., Gasteiger, J., Garhammer, M., and Seefeldner, M.: Depolarization ratio profiling at several wavelengths in pure Saharan dust during Samum 2006, *Tellus B*, 61, 165–179, 2009.

Gasteiger, J., Groß, S., Freudenthaler, V., and Wiegner, M.: Volcanic ash from Iceland over Munich: mass concentration retrieved from ground-based remote sensing measurements, *Atmos. Chem. Phys.*, 11, 2209–2223, doi:10.5194/acp-11-2209-2011, 2011.

- Gimmestad, G.: Reexamination of depolarization in lidar measurements, *Appl. Opt.*, 47, 3795–3802, 2008.
- Glen, A. and Brooks, S. D.: A new method for measuring optical scattering properties of atmospherically relevant dusts using the Cloud Aerosol Spectrometer Polarization (CASPOL) instrument, *Atmos. Chem. Phys. Discuss.*, 12, 22415–22449, doi:10.5194/acpd-12-22415-2012, 2012.
- Groß, S., Tesche, M., Freudenthaler, V., Toledano, C., Wiegner, M., Ansmann, A., Althausen, D., and Seefeldne, M.: Characterization of Saharan dust, marine aerosols and mixtures of biomass-burning aerosols and dust by means of multi-wavelength depolarization and Raman lidar measurements during SAMUM 2, *Tellus B*, 63, 706–724, 2011.
- Harris-Hobbs, R. L. and Cooper, W. A.: Field evidence supporting quantitative predictions of secondary ice production rates, *J. Atmos. Sci.*, 44, 1071–1082, doi:10.1175/1520-0469, 1987.
- Bay Hasager, C., Birmili, W., Pappalardo, G., and Prata, F.: Atmospheric implications of the volcanic eruptions of Eyjafjallajökull, Iceland, special issue, 2010.
- Hess, M., Koepke, P., and Schult I.: Optical properties of aerosols and clouds: the software package OPAC, *B. Am. Meteor. Soc.*, 79, 831–844, 1998.
- IPCC: Climate Change 2007: The Physical Science Basis. Contribution of Working Group I to 5 the Fourth Assessment Report of the Intergovernmental Panel on Climate Change, Cambridge, UK and New York, NY, USA, 996 pp., 2007.
- Kaaden, N., Massling, A., Schladitz, A., Müller, T., Kandler, K., Schütz, L., Weinzierl, B., Petzold, A., Tesche, M., Leinert, S., Deutscher, C., Ebert, M., Weinbruch, S., and Wiedensohler, A.: State of mixing, shape factor, number size distribution, and hygroscopic growth of the Saharan anthropogenic and mineral dust aerosol at Tinfou, Morocco, *Tellus B*, 61, 51–63, 2009.
- Kandler, K., Lieke, K., Benker, N., Emmel, C., Küpper, M., Müller-Ebert D., Ebert, M., Scheuvsen D., Schladitz, A., Schütz, L., and Weinbruch S.: Electron microscopy of particles collected at Praia, Cape Verde, during the Saharan mineral dust experiment: particle chemistry, shape, mixing state and complex refractive index, *Tellus B*, 63, 475–496, 2011.
- Kahnert, M.: Numerical methods in electromagnetic scattering theory. *J. Quant. Spec. Rad. Transf.*, 79–80, 775–824, 2003.
- Kahnert, M.: The T-matrix code Tsym for homogeneous dielectric particles with finite symmetries. *J. Quant. Spec. Rad. Transf.*, doi:10.1016/j.jqsrt.2012.12.019, 2013.

Retrieving volcanic, desert dust, and sea-salt particle properties

G. David et al.

[Title Page](#)[Abstract](#)[Introduction](#)[Conclusions](#)[References](#)[Tables](#)[Figures](#)[⏪](#)[⏩](#)[◀](#)[▶](#)[Back](#)[Close](#)[Full Screen / Esc](#)[Printer-friendly Version](#)[Interactive Discussion](#)

Retrieving volcanic, desert dust, and sea-salt particle properties

G. David et al.

Title Page

Abstract

Introduction

Conclusions

References

Tables

Figures

⏪

⏩

◀

▶

Back

Close

Full Screen / Esc

Printer-friendly Version

Interactive Discussion



- Kahnert, M., Nousiainen, T., and Räisänen P.: Mie simulations as an error source in mineral aerosol radiative forcing calculations, *Q. J. R. Meteorol. Soc.*, 133, 299–307, 2007.
- Lindqvist H., Nousiainen, T., Zubko, E., and Munoz, O.: Optical modeling of vesicular volcanic ash particles, *J. Quant. Spec. Rad. Transf.*, 112, 1871–1880, 2011.
- 5 Mallet, M., Roger, J. C., Despiiau, S., Putaud, J. P., and Dubovik, O.: A study of the mixing state of black carbon in urban zone, *J. Geophys. Res.*, 109, D04202, doi:10.1029/2003JD003940, 2004.
- Mather, T. A., Pyle, D. M., and Oppenheimer, C.: Tropospheric volcanic aerosol, volcanism and the Earth's atmosphere, *Geophys. Monograph*, 139, doi:10.129/10.1029/GM139, 189–212, 10
2003.
- Merikallio, S., Lindqvist, H., Nousiainen, T., and Kahnert, M.: Modelling light scattering by mineral dust using spheroids: assessment of applicability, *Atmos. Chem. Phys.*, 11, 5347–5363, doi:10.5194/acp-11-5347-2011, 2011.
- Miffre, A., Abou Chacra, M., Geffroy, S., Rairoux, P., Soulhac, L., Perkins, R. J., and Frejafon, E.: 15
Aerosol load study in urban area by Lidar and numerical model, *Atmos. Environ.* 44, 1152–1161, 2010.
- Miffre A., David, G., Thomas, B., and Rairoux, P.: Atmospheric non-spherical particles optical properties from UV-polarization lidar and scattering matrix, *Geophys. Res. Lett.*, 38, L16804, doi:10.1029/2011GL048310, 2011.
- 20 Miffre, A., David, G., Thomas, B., Rairoux, P., Fjaeraa, A. M., Kristiansen, N. I., and Stohl A.: Volcanic aerosol optical properties and phase partitioning behavior after long-range advection characterized by UV-Lidar measurements, *Atmos. Environ.* 48, 76–84, 2012a.
- Miffre A., David, G., Thomas, B., Abou Chacra, M., and Rairoux, P.: Interpretation of accurate UV-Polarization Lidar measurements: application to volcanic ash number concentration 25
retrieval, *J. Atmos. Ocean. Tech.*, 29, 558–568, 2012b.
- Mishchenko M. I.: Electromagnetic scattering by nonspherical particles: a tutorial review, *J. Quant. Spec. Rad. Transf.*, 110, 808–832, 2009.
- Mishchenko, M. I. and Hovenier, J. W.: Depolarization of light backscattered by randomly oriented non spherical particles, *Opt. Lett.*, 20, 1356–1359, doi:10.1364/OL.20.001356, 1995.
- 30 Mishchenko, M. I. and Travis L. D.: Capabilities and limitations of a current Fortran implementation of the T-matrix method for randomly oriented rotationally symmetric scatterers, *J. Quant. Spectrosc. Radiat. Transf.*, 60, 309–324, 1998.

**Retrieving volcanic,
desert dust, and
sea-salt particle
properties**

G. David et al.

[Title Page](#)[Abstract](#)[Introduction](#)[Conclusions](#)[References](#)[Tables](#)[Figures](#)[⏪](#)[⏩](#)[◀](#)[▶](#)[Back](#)[Close](#)[Full Screen / Esc](#)[Printer-friendly Version](#)[Interactive Discussion](#)

- Mishchenko, M. I., Wiscombe, W. J., Hovenier, J. W. and Travis, L. D.: Overview of scattering by nonspherical particles. In: *Light Scattering by Nonspherical Particles*, edited by: Mishchenko, M. I., Hovenier, J. W., and Travis L. D., Academic Press, San Diego, 29–60, 2000.
- 5 Mishchenko, M. I., Travis, L. D., and Lacis, A. A.: *Scattering, Absorption and Emission of Light by Small Particles*, 3rd edn., Cambridge University Press, UK, 2002.
- Mishchenko, M. I., Lacis, A. A., Carlson, B. E., and Travis L. D.: Nonsphericity of dust-like tropospheric aerosols: implications for aerosol remote sensing and climate modeling, *Geophys. Res. Lett.*, 22, 1077–1080, doi:10.1029/95GL00798, 1995.
- 10 Mueller, D., Wandinger, U., Althausen, D., and Fiebig, M.: Comprehensive particle characterization from three-wavelength Raman-lidar observations, *Appl. Opt.*, 40, 4863–4869, 2001.
- Muñoz, O., Volten, H., Hovenier, J. W., Veihelmann, B., van der Zande, W. J., Waters, L. B. F. M., and Rose, W. I.: Scattering matrices of volcanic ash particles of Mount St Helens, Redoubt, and Mount Spurr volcanoes. *J. Geophys. Res.*, 109, D16201, doi:10.1029/2004JD004684, 2004.
- 15 Murayama, T., Okamoto, H., Kaneyasu, N., Kamataki, H., and Miura, K.: Application of lidar depolarization measurement in the atmospheric boundary layer: effects of dust and sea-salt particles, *J. Geophys. Res.*, 104, 31781–31792, doi:10.1029/1999JD900503, 1999.
- Nicolet, M., Schnaiter, M., and Stetzer, O.: Circular depolarization ratios of single water droplets and finite ice circular cylinders: a modeling study, *Atmos. Chem. Phys.*, 12, 4207–4214, doi:10.5194/acp-12-4207-2012, 2012.
- 20 Nishizawa T., Sugimoto, N., Matsui, I., Shimizu, A., and Okamoto, H.: Algorithms to retrieve optical properties of three component aerosols from two-wavelength backscatter and one-wavelength polarization lidar measurements considering nonsphericity of dust, *J. Quant. Spec. Rad. Transf.*, 112, 254–267, 2011.
- 25 Nousiainen, T.: Optical modeling of mineral dust particles: a review, *J. Quant. Spec. Rad. Transf.*, 110, 1261–1279, 2009.
- Nousiainen T. and Vermeulen, K.: Comparison of measured single-scattering matrix of feldspar particles with T-matrix simulations using spheroids, *J. Quant. Spec. Rad. Transf.*, 79, 1031–1042, 2003.
- 30 Nousiainen, T., Kahnert, M., and Veihelmann, B.: Light scattering modeling of small feldspar aerosol particles using polyhedral prisms and spheroids, *J. Quant. Spec. Rad. Transf.*, 101, 471–487, 2006.

Retrieving volcanic, desert dust, and sea-salt particle properties

G. David et al.

Title Page

Abstract

Introduction

Conclusions

References

Tables

Figures

⏪

⏩

◀

▶

Back

Close

Full Screen / Esc

Printer-friendly Version

Interactive Discussion



- Nousiainen, T., Zubko, E., Lindqvist, H., Kahnert, M., and Tyynel, J.: Comparison of scattering by different nonspherical, wavelength-scale particles, *J. Quant. Spec. Rad. Transf.*, 113, 2391–2405, 2012.
- O'Dowd C., Smith, M. H., Consterdine, I. E., and Lowe, J. A.: Marine aerosol, sea salt, and the marine sulfur cycle: a short review, *Atmos. Environ.*, 31, 73–80, 1997.
- 5 Ovadnevaite, J., Ceburnis, D., Plauskaite-Sukiene, K., Modini, R., Dupuy, R., Rimselyte, I., Ramonet, R., Kvietkus, K., Ristovski, Z., Berresheim, H., and O'Dowd, C.: Volcanic sulfate and arctic dust plumes over the North Atlantic Ocean, *Atmos. Environ.*, 43, 4968–4974, 2009.
- 10 Ramaswamy, V., Chanin, M. L., Angell, J., Barnett, J., Gaffen, D., Gelman, M., Keckhut, P., Koshelkov, Y., Labitzke, K., Lin, J.-J. R., O'Neill, A., Nash, J., Randel, W., Rood, R., Shine, K., Shiotani, M., and Swinbank, R.: Stratospheric temperature trends: observations and model simulations, *Rev. Geophys.*, 39, 71–122, 2001.
- Randriamiarisoa, H., Chazette, P., Couvert, P., Sanak, J., and Mégie, G.: Relative humidity impact on aerosol parameters in a Paris suburban area, *Atmos. Chem. Phys.*, 6, 1389–1407, doi:10.5194/acp-6-1389-2006, 2006.
- 15 Riccobono, F., Rondo, L., Sipilä, M., Barmet, P., Curtius, J., Dommen, J., Ehn, M., Ehrhart, S., Kulmala, M., Kürten, A., Mikkilä, J., Paasonen, P., Petäjä, T., Weingartner, E., and Baltensperger, U.: Contribution of sulfuric acid and oxidized organic compounds to particle formation and growth, *Atmos. Chem. Phys.*, 12, 9427–9439, doi:10.5194/acp-12-9427-2012, 2012.
- Robock, A.: Volcanic eruptions and climate, *Rev. Geophys.*, 38, 191–219, 2000.
- Sakäi, T., Nagai, T., Zaizen, Y., and Mano, Y.: Backscattering linear depolarization ratio measurements of mineral, sea-salt, and ammonium sulfate particles simulated in a laboratory chamber, *Appl. Opt.*, 23, 4441–4449, 2010.
- 25 Sasano, Y. and Browell, E. V.: Light scattering characteristic of various aerosol types derived from multiple wavelength lidar observations, *Appl. Opt.*, 28, 1670–1679, 1989.
- Sassen, K., Zhu, J., Webley, P., Dean, K., and Cobb, P.: Volcanic ash plume identification using polarization lidar: Augustine eruption, Alaska, *Geophys. Rev. Lett.*, 34, L08803, doi:10.1029/2006GL027237, 2007.
- 30 Shimizu, A., Sugimoto, N., Matsui, I., Arai, K., Uno, I., Murayama, T., Kagawa, N., Aoki, K., Uchiyama, A., and Yamazaki, A.: Continuous observations of Asian dust and other aerosols

Retrieving volcanic, desert dust, and sea-salt particle properties

G. David et al.

Title Page

Abstract

Introduction

Conclusions

References

Tables

Figures

⏪

⏩

◀

▶

Back

Close

Full Screen / Esc

Printer-friendly Version

Interactive Discussion

by polarization lidars in China and Japan during ACE-Asia. *J. Geophys. Res.*, 109, D19S17, doi:10.1029/2002JD003253, 2004.

Shettle, E. P. and Fenn, R. W.: Models for the Aerosols of the Lower Atmosphere and the Effects of Humidity Variations on Their Optical Properties, AFGL-TR-79-0214, Environmental Research Papers. No. M61979, 1979.

Schnaiter, M., Büttner, S., Möhler, O., Skrotzki, J., Vragel, M., and Wagner, R.: Influence of particle size and shape on the backscattering linear depolarisation ratio of small ice crystals – cloud chamber measurements in the context of contrail and cirrus microphysics, *Atmos. Chem. Phys.*, 12, 10465–10484, doi:10.5194/acp-12-10465-2012, 2012.

Schumann, U., Weinzierl, B., Reitebuch, O., Schlager, H., Minikin, A., Forster, C., Baumann, R., Sailer, T., Graf, K., Mannstein, H., Voigt, C., Rahm, S., Simmet, R., Scheibe, M., Lichtenstern, M., Stock, P., Rüba, H., Schäuble, D., Tafferner, A., Rautenhaus, M., Gerz, T., Ziereis, H., Krautstrunk, M., Mallaun, C., Gayet, J.-F., Lieke, K., Kandler, K., Ebert, M., Weinbruch, S., Stohl, A., Gasteiger, J., Groß, S., Freudenthaler, V., Wiegner, M., Ansmann, A., Tesche, M., Olafsson, H., and Sturm, K.: Airborne observations of the Eyjafjalla volcano ash cloud over Europe during air space closure in April and May 2010, *Atmos. Chem. Phys.*, 11, 2245–2279, doi:10.5194/acp-11-2245-2011, 2011.

Stiller, G. P., Kiefer, M., Eckert, E., von Clarmann, T., Kellmann, S., García-Comas, M., Funke, B., Leblanc, T., Fetzer, E., Froidevaux, L., Gomez, M., Hall, E., Hurst, D., Jordan, A., Kämpfer, N., Lambert, A., McDermid, I. S., McGee, T., Miloshevich, L., Nedoluha, G., Read, W., Schneider, M., Schwartz, M., Straub, C., Toon, G., Twigg, L. W., Walker, K., and Whiteman, D. N.: Validation of MIPAS IMK/IAA temperature, water vapor, and ozone profiles with MOHAVE-2009 campaign measurements, *Atmos. Meas. Tech.*, 5, 289–320, doi:10.5194/amt-5-289-2012, 2012.

Sugimoto, N. and Lee, C. H.: Characteristics of dust aerosols inferred from lidar depolarization measurements at two wavelengths, *Appl. Opt.*, 45, 7468–7474, 2006.

Sugimoto, N., Matsui, I., Shimizu, A., Uno, I., Asai, K., Endoh, T., and Nakajima, T.: Observation of dust and anthropogenic aerosol plumes in the Northwest Pacific with a two-wavelength polarization lidar on board the research vessel Mirai, *Geophys. Res. Lett.* 29, 7-1–7-4, doi:10.1029/2002GL015112, 2002.

Tesche, M., Ansmann, A., Müller, D., Althausen, D., Engelmann, R., Freudenthaler, V., and Groß, S.: Vertically resolved separation of dust and smoke over Cape Verde using multi-

Retrieving volcanic, desert dust, and sea-salt particle properties

G. David et al.

Title Page

Abstract

Introduction

Conclusions

References

Tables

Figures

⏪

⏩

◀

▶

Back

Close

Full Screen / Esc

Printer-friendly Version

Interactive Discussion



wavelength Raman and polarization lidars during Saharan Mineral Dust Experiment 2008, *J. Geophys. Res.*, 114, D13202, doi:10.1029/2009JD011862, 2009.

Thomas, B., Miffre, A., David, G., Cariou, J. P., and Rairoux, P.: Remote sensing of trace gases with optical correlation spectroscopy and lidar: theoretical and numerical approach, *Appl. Phys. B*, 108, 689–702, 2012.

Vernier, J.-P., Pommereau, J.-P., Thomason, L. W., Pelon, J., Garnier, A., Deshler, T., Jumelet, J., and Nielsen, J. K.: Overshooting of clean tropospheric air in the tropical lower stratosphere as seen by the CALIPSO lidar, *Atmos. Chem. Phys.*, 11, 9683–9696, doi:10.5194/acp-11-9683-2011, 2011.

Veselovskii, I., Dubovik, O., Kolgotin, A., Lapyonok, T., Di Girolamo, P., Summa, D., Whiteman, D. N., Mishchenko, M., and Tanré, D.: Application of randomly oriented spheroids for retrieval of dust particle parameters from multiwavelength lidar measurements, *J. Geophys. Res.*, 115, D21203, doi:10.1029/2010JD014139, 2010.

Volten, H., Muñoz, O., Rol, E., de Haan, J. F., Vassen, W., Hovenier, J. W., Muinonen, K., and Nousiainen, T.: Scattering matrices of mineral aerosol particles at 441.6 and 632.8 nm. *J. Geophys. Res.*, 106, 17375–17401, doi:10.1029/2001JD900068, 2001.

Wiegner, M., Gasteiger, J., Kandler, K., Weinzierl, B., Rasp, K., Esselborn, M., Freudenthaler, V., Heese, B., Toledano, C., Tesche, M., and Althausen, D.: Numerical simulations of optical properties of Saharan dust aerosols with emphasis on lidar applications, *Tellus B*, 61, 180–194, 2009.

Wiegner, M., Groß, S., Freudenthaler, V., Schnell, F., and Gasteiger, J.: The May/June 2008 Saharan dust event over Munich: intensive aerosol parameters from lidar measurements, *J. Geophys. Res.*, 116, D23213, doi:10.1029/2011JD016619, 2011.

Winker, D. M. and Osborn, M. T.: Preliminary analysis of observations of the Pinatubo volcanic cloud with a polarization-sensitive lidar, *Geophys. Res. Lett.*, 19, 171–174, 1992.

Winker, D. M., Vaughan, M. A., Omar, A., Hu, Y., Powell, K. A., Liu, Z., Hunt, W. H., and Young, S. A.: Overview of the CALIPSO Mission and CALIOP data processing algorithms, *J. Atmos. Ocean. Tech.*, 26, 2310–2323, 2009.

Winker, D. M., Pelon, J., Coakley Jr., J. A., Ackerman, S. A., Charlson, R. J., Colarco, P. R., Flamant, P., Fu, Q., Hoff, R. M., Kittaka, C., Kubar, T. L., Le Treut, H., McCormick, M. P., Megie, G., Poole, L., Powell, K., Trepte, C., Vaughan, M. A., and Wielicki, B. A.: THE CALIPSO mission global 3-D view of aerosols and clouds, *Bull. Am. Meteor. Soc.*, 9, 1211–1229, 2010.

Wise M. E., Biskos, G., Martin, S. T., Russell, L. M., and Buseck, P. R.: Phase transitions of single salt particles studied using a transmission electron microscope with an environmental cell, *Aerosol Sci. Tech.*, 39, 849–856, 2005.

Zhang, D.: Effect of sea salt on dust settling to the ocean, *Tellus B*, 60, 641–646, 2008.

ACPD

13, 1891–1947, 2013

Retrieving volcanic, desert dust, and sea-salt particle properties

G. David et al.

Title Page

Abstract

Introduction

Conclusions

References

Tables

Figures



Back

Close


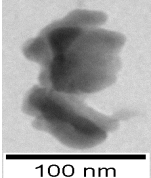
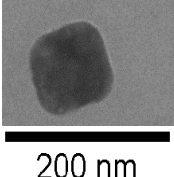
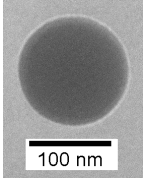
Full Screen / Esc

Printer-friendly Version

Interactive Discussion



Table 1. Electron microscope images of desert dust particles, sea-salt (ss) particles and water-soluble (ws) particles (an ammonium sulphate particle is observed) taken at ILM. In this paper, ws-particles are assumed spherical (s-particles). For volcanic ash, in the absence of measurement at the ILM, the image has been provided by O. Muñoz from Mount Spurr volcanic eruption.

Particle type	Label	Literature references	Electron microscope image
Volcanic ash	(ash)	Winker and Osborn (1992) Mather et al. (2003), Muñoz et al. (2004), Sassen et al. (2007) Schumann et al. (2011), Eyjaflajökull ACP SI (Bay Hasager et al., 2012) Lindqvist et al., (2011), Miffre et al. (2012a, b)	
Desert dust	(dust)	Shimizu et al., (2004) Mallet et al. (2004) Kaaden et al. (2009) Veselovskii et al. (2010) Ansmann et al. (2011) Di Girolamo et al. (2012) Nishizawa et al. (2011) Nousiainen (2009)	
Sea-salt	(ss)	Shettle et al., (1979) O'Dowd et al. (1997) Murayama et al. (1999) Wise et al. (2005) Zhang (2008) Sakai et al. (2010)	
Water-soluble	(ws)	Hess et al., (1998) O'Dowd et al. (1997) Di Girolamo et al. (2012) Nishizawa et al. (2011)	

Retrieving volcanic, desert dust, and sea-salt particle properties

G. David et al.

Title Page

Abstract

Introduction

Conclusions

References

Tables

Figures

⏪

⏩

◀

▶

Back

Close

Full Screen / Esc

Printer-friendly Version

Interactive Discussion

Retrieving volcanic, desert dust, and sea-salt particle properties

G. David et al.

Table 2. Input parameters used in the numerical T-matrix simulation on ns-particles (ash, dust, sea-salt): m -complex refractive index at the Lidar wavelengths (UV, $\lambda_1 = 355$ nm; VIS, $\lambda_2 = 532$ nm), size parameter range, modelled shape, aspect ratios values and literature reference for the m -refractive index. The discrete set of x -values is $x = 0.01, 0.02, 0.1, 0.25, 0.5, 1$; step of 1 for $x = 1$ to 10, step of 2 for $x = 10$ to 30, 35, 40, then 45, 50.

Ns-particle	Label	m	X	Shape	ε	Reference
Volcanic ash	(ash)	$1.54 - 0.0054i$ (UV, VIS)	0.01 to 50	Spheroid	1.2, ..., 2.6	Muñoz et al. (2004)
Desert dust	(dust)	$1.57 - 0.007i$ (UV, VIS)	0.01 to 50	Spheroid	1.2, ..., 2.6	Kandler et al. (2011)
Sea-salt	(ss)	$1.51 - 0.0004i$ (UV) $1.50 - 0.00001i$ (VIS)	0 to 20	Cubic	1.2, ..., 2.6	Shettle et al. (1979)

Title Page

Abstract

Introduction

Conclusions

References

Tables

Figures

⏪

⏩

◀

▶

Back

Close

Full Screen / Esc

Printer-friendly Version

Interactive Discussion



Retrieving volcanic, desert dust, and sea-salt particle properties

G. David et al.

Table 3. Results of the T-matrix simulations: depolarization ratios δ_{ns} averaged over the corresponding PSD, cross-polarized Angstrom exponents $\dot{A}_{\text{ns},\perp}$ ($\lambda_1 = 355$ nm, $\lambda_2 = 532$ nm) and extinction-to-backscatter ratios S_{ns} , for each ns-particle component: volcanic ash, desert dust, sea-salt (ss) at $\lambda_1 = 355$ nm (UV), at $\lambda_2 = 532$ nm (VIS).

Ns-particles	Label	$\delta_{\text{ns}}(\text{UV})$ [%]	$\delta_{\text{ns}}(\text{VIS})$ [%]	$\dot{A}_{\text{ns},\perp}$ ($\lambda_1 = \text{UV}, \lambda_2 = \text{VIS}$)	$S_{\text{ns}}(\text{UV})$ [sr]	$S_{\text{ns}}(\text{VIS})$ [sr]
Volcanic ashes	(ash)	26.7	27.2	0.015	53.6	56.3
Desert dust	(dust)	0.196	0.143	1.376	65.7	61.3
Sea-salt	(ss)	0.159	0.162	-0.488	18.8	20.1

[Title Page](#)
[Abstract](#)
[Introduction](#)
[Conclusions](#)
[References](#)
[Tables](#)
[Figures](#)
[⏪](#)
[⏩](#)
[◀](#)
[▶](#)
[Back](#)
[Close](#)
[Full Screen / Esc](#)
[Printer-friendly Version](#)
[Interactive Discussion](#)


Retrieving volcanic, desert dust, and sea-salt particle properties

G. David et al.

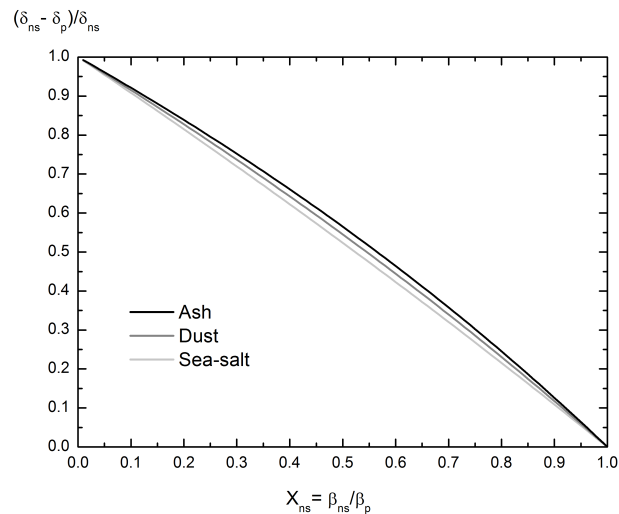


Fig. 1. Systematic bias on δ_{ns} when assuming δ_p equals to δ_{ns} for $\delta_{ns} = 10\%$ as for sea-salt particles (light gray), $\delta_{ns} = 20\%$, as for desert dust particles (dark gray), $\delta_{ns} = 30\%$, as for volcanic ashes (black).

Title Page

Abstract

Introduction

Conclusions

References

Tables

Figures

◀

▶

◀

▶

Back

Close

Full Screen / Esc

Printer-friendly Version

Interactive Discussion



Retrieving volcanic, desert dust, and sea-salt particle properties

G. David et al.

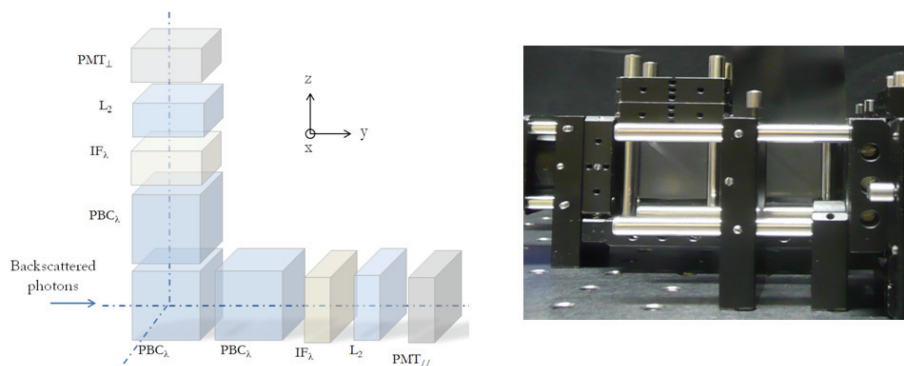


Fig. 2. Left: 3-D view of a Lyon λ -polarization channel: each polarization channel is composed of two polarization beamsplitter cubes (PBC), one interference filter (IF) and a collecting system (lens + photomultiplier tube PMT). Right: photograph of the UV cross-polarized Lidar polarization channel composed of two PBC. The subscripts // and \perp are defined with respect to the laser incident polarization, respectively corresponding to the co- and cross-polarized polarization Lidar channels.

[Title Page](#)
[Abstract](#)
[Introduction](#)
[Conclusions](#)
[References](#)
[Tables](#)
[Figures](#)
[◀](#)
[▶](#)
[◀](#)
[▶](#)
[Back](#)
[Close](#)
[Full Screen / Esc](#)
[Printer-friendly Version](#)
[Interactive Discussion](#)

Retrieving volcanic, desert dust, and sea-salt particle properties

G. David et al.

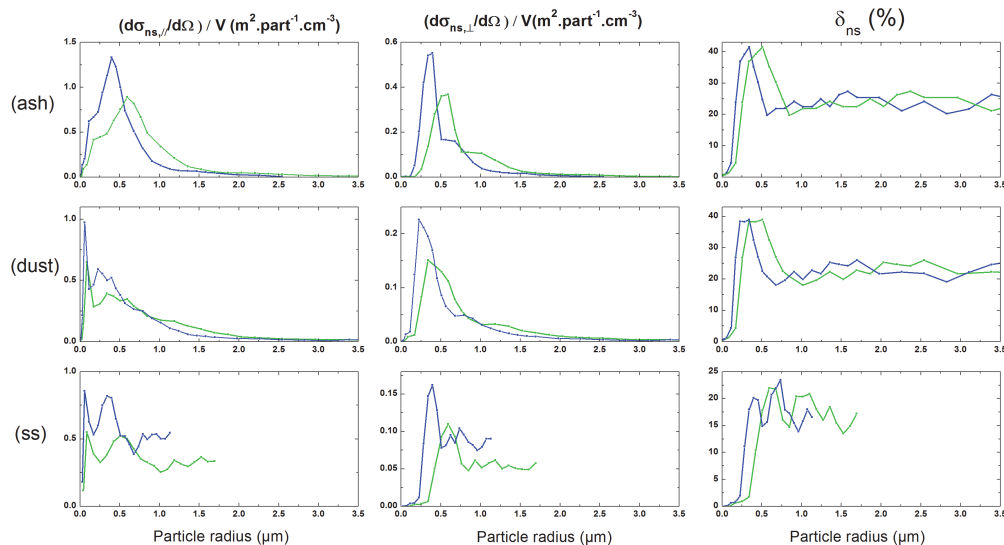


Fig. 3. Ns-particle backscattering cross-section $(d\sigma/d\Omega)_{ns,\parallel}$ and $(d\sigma/d\Omega)_{ns,\perp}$ per particle volume and ns-particle depolarization ratio δ_{ns} as a function of the particle radius r in the UV (blue, $\lambda_1 = 355$ nm) and in the VIS (green, $\lambda_2 = 532$ nm) for each ns-particle type (ash, dust and sea-salt (ss)).

[Title Page](#)
[Abstract](#)
[Introduction](#)
[Conclusions](#)
[References](#)
[Tables](#)
[Figures](#)
[⏪](#)
[⏩](#)
[◀](#)
[▶](#)
[Back](#)
[Close](#)
[Full Screen / Esc](#)
[Printer-friendly Version](#)
[Interactive Discussion](#)

Retrieving volcanic, desert dust, and sea-salt particle properties

G. David et al.

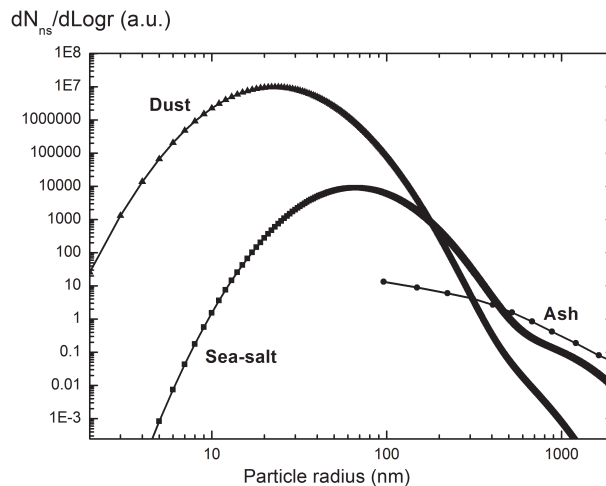


Fig. 4. Ns-particle size distributions (PSD) for volcanic ash (Muñoz et al., 2004), desert dust (Mallet et al., 2004) and sea-salt particles (ss, O'Dowd et al., 1997).

[Title Page](#)[Abstract](#)[Introduction](#)[Conclusions](#)[References](#)[Tables](#)[Figures](#)[⏪](#)[⏩](#)[◀](#)[▶](#)[Back](#)[Close](#)[Full Screen / Esc](#)[Printer-friendly Version](#)[Interactive Discussion](#)

Retrieving volcanic, desert dust, and sea-salt particle properties

G. David et al.

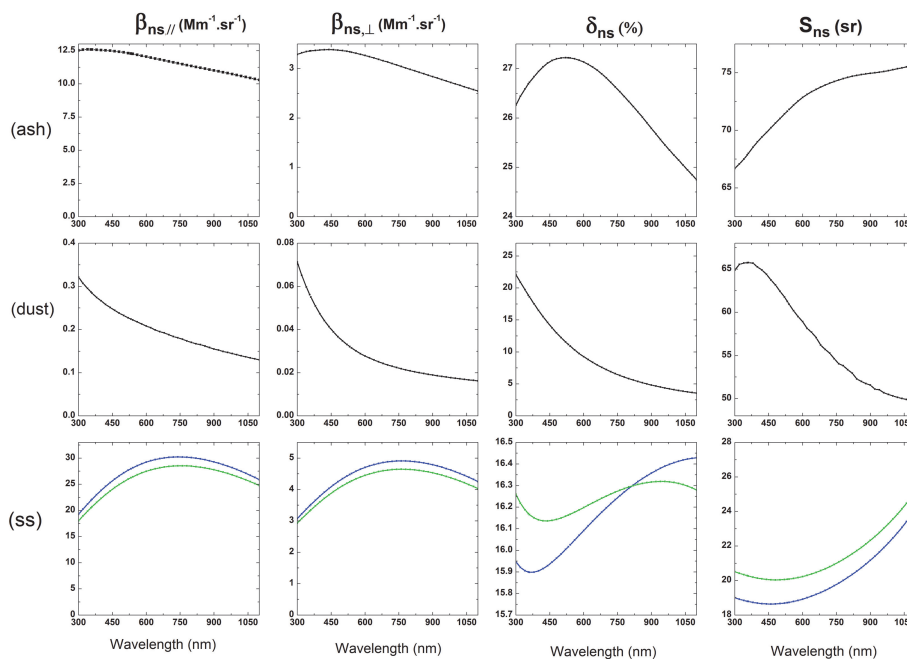


Fig. 5. Ns-particle backscattering coefficients, particle depolarization ratios δ_{ns} and extinction-to-backscatter ratios S_{ns} as a function of the λ -wavelength, for each ns-particles type: volcanic ash, desert dust and sea-salt (ss).

[Title Page](#)
[Abstract](#)
[Introduction](#)
[Conclusions](#)
[References](#)
[Tables](#)
[Figures](#)
[⏪](#)
[⏩](#)
[◀](#)
[▶](#)
[Back](#)
[Close](#)
[Full Screen / Esc](#)
[Printer-friendly Version](#)
[Interactive Discussion](#)

Retrieving volcanic, desert dust, and sea-salt particle properties

G. David et al.

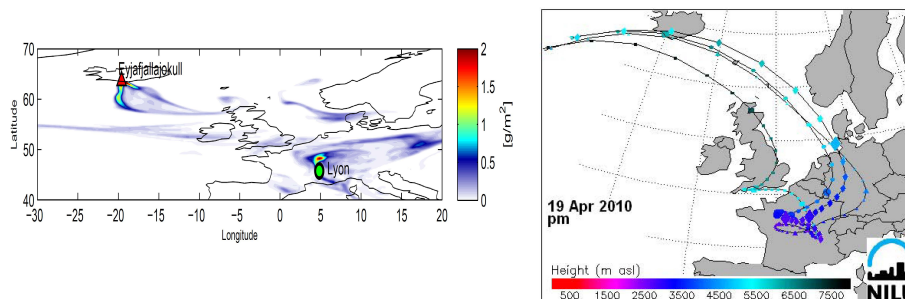


Fig. 6. Evidence of the presence of volcanic ash over Lyon on 19 April at 19:00 UTC. Left: NILU FLEXPART ash particle numerical dispersion model for 19 April 2010 at 19:00 UTC. Right: NILU FLEXTRA 7-days air mass back-trajectories on 19 April at 18:00 UTC (2 km, triangles; 3 km, circles; 5 km altitude, squares) and at 12:00 UTC (3 km, diamonds).

Title Page

Abstract

Introduction

Conclusions

References

Tables

Figures

◀

▶

◀

▶

Back

Close

Full Screen / Esc

Printer-friendly Version

Interactive Discussion

Retrieving volcanic, desert dust, and sea-salt particle properties

G. David et al.

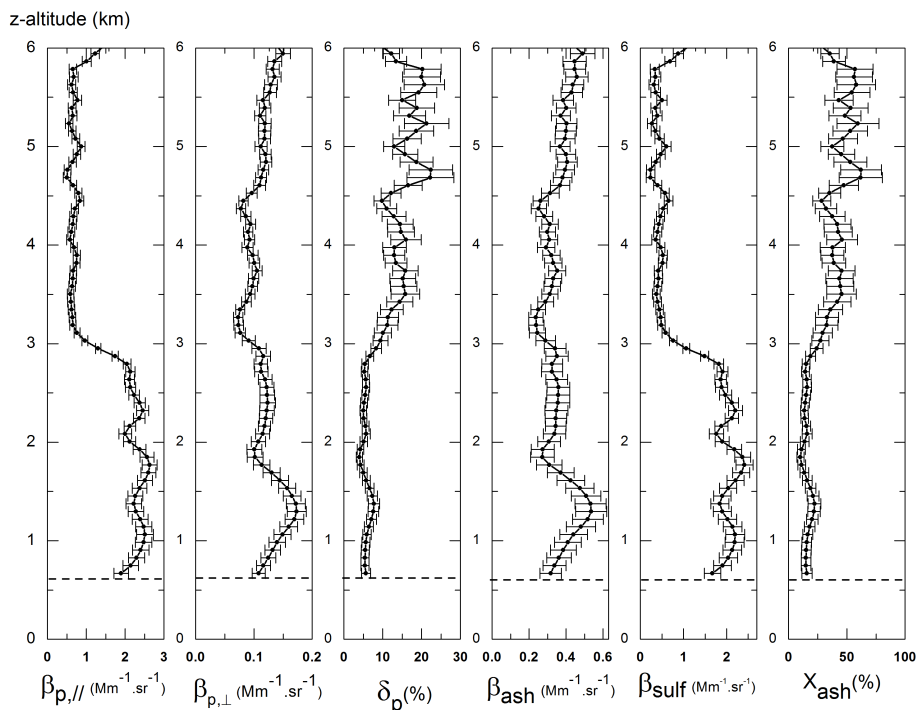


Fig. 7. Vertical profiles of backscattering coefficients $\beta_{p,||}$, $\beta_{p,\perp}$, depolarization ratio δ_p , retrieved β_{ash} and β_{sulf} coefficients and ash particle backscattering fraction $X_{\text{ash}} = \beta_{\text{ash}}/\beta_p$ in the mixed {ash, sulphate} particle cloud on 19 April 2010 at 19:00 UTC at Lyon. The experiment is performed in the UV ($\lambda = 355 \text{ nm}$).

[Title Page](#)
[Abstract](#)
[Introduction](#)
[Conclusions](#)
[References](#)
[Tables](#)
[Figures](#)
[◀](#)
[▶](#)
[◀](#)
[▶](#)
[Back](#)
[Close](#)
[Full Screen / Esc](#)
[Printer-friendly Version](#)
[Interactive Discussion](#)

Retrieving volcanic, desert dust, and sea-salt particle properties

G. David et al.

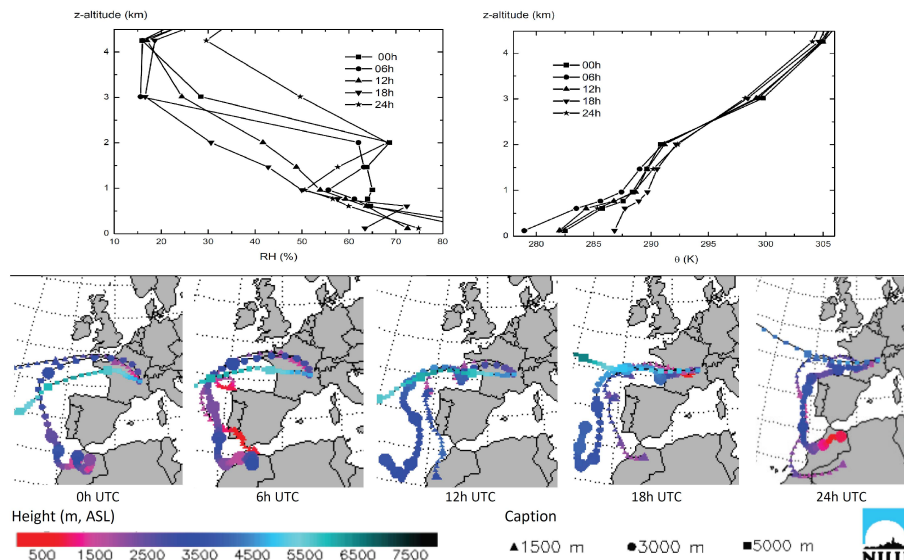


Fig. 8. Upper panel: Relative humidity (RH) and potential temperature (θ) vertical profiles on 18 October 2011 at Lyon (Météo France). Lower panel: FLEXTRA 7-days air mass back-trajectories showing evidence of sea-salt and dust particles content in the Lyon atmosphere on 18 October 2011.

[Title Page](#)
[Abstract](#)
[Introduction](#)
[Conclusions](#)
[References](#)
[Tables](#)
[Figures](#)
[⏪](#)
[⏩](#)
[◀](#)
[▶](#)
[Back](#)
[Close](#)
[Full Screen / Esc](#)
[Printer-friendly Version](#)
[Interactive Discussion](#)

Retrieving volcanic, desert dust, and sea-salt particle properties

G. David et al.

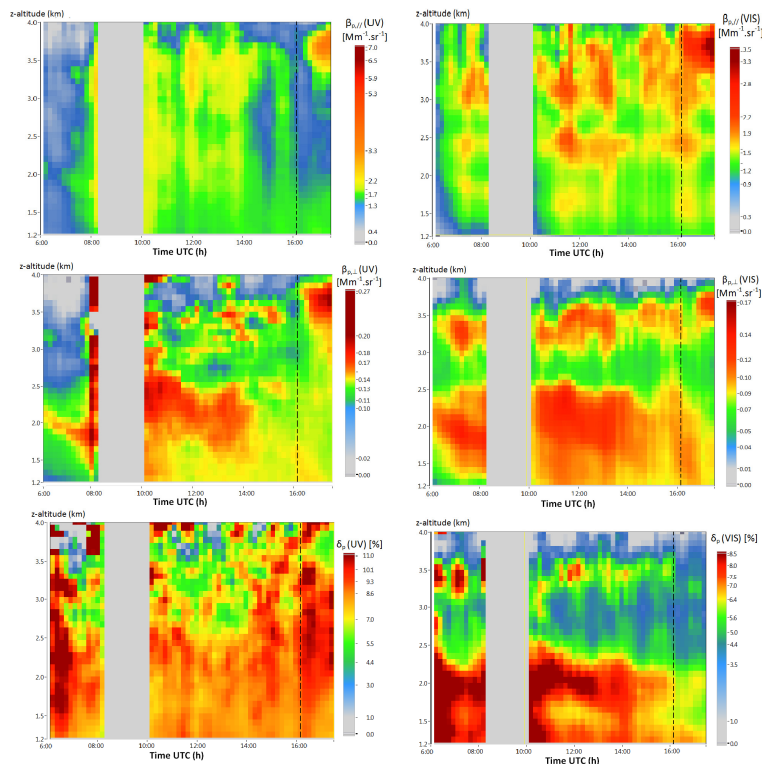


Fig. 9. Time-altitude maps of $\beta_{p, //}$, $\beta_{p, \perp}$ and δ_p in the UV ($\lambda_1 = 355$ nm, left three vertical panels) and in the VIS ($\lambda_2 = 532$ nm, right three vertical panels) on 18 October 2011 at Lyon. The grey band corresponds to clouds which prevented retrieving the $\beta_{p, //}$, $\beta_{p, \perp}$, δ_p -coefficients. Dashed lines correspond to Fig. 10-case study, at 16:15 UTC.

Title Page

Abstract Introduction

Conclusions References

Tables Figures

⏪ ⏩

◀ ▶

Back Close

Full Screen / Esc

Printer-friendly Version

Interactive Discussion



Retrieving volcanic,
desert dust, and
sea-salt particle
properties

G. David et al.

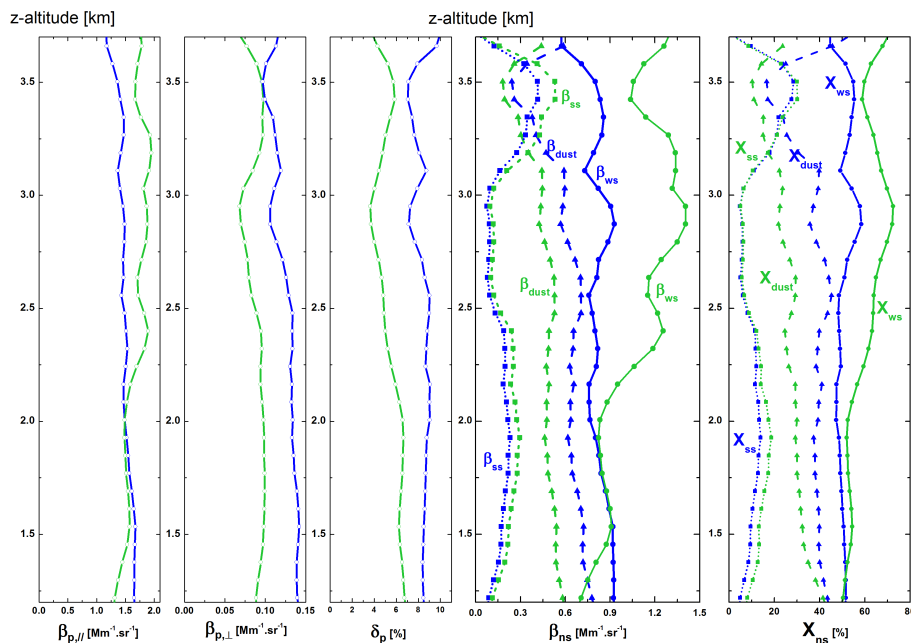


Fig. 10. Vertical profiles of $\beta_{p,||}$, $\beta_{p,\perp}$, δ_p , β_{dust} , β_{ss} and β_{ws} and fraction of ns-particles (dust, ss, ws) in the three-component mixture { dust, sea-salt, water-soluble } on 18 October 2011 at 16:15 UTC at Lyon₁ (France), addressed in the UV (blue) at $\lambda_1 = 355$ nm and in the VIS (green) at $\lambda_2 = 532$ nm. To ease the reading, error bars are not plotted on this graph.

Title Page

Abstract

Introduction

Conclusions

References

Tables

Figures

◀

▶

◀

▶

Back

Close

Full Screen / Esc

Printer-friendly Version

Interactive Discussion